UNIVERSITY OF TWENTE.

Faculty of Electrical Engineering, Mathematics & Computer Science
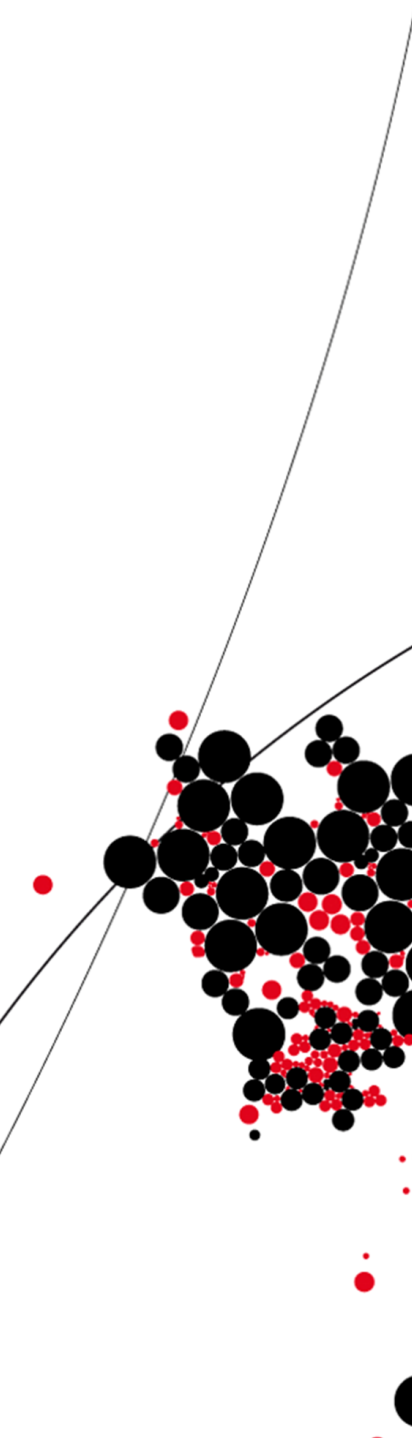
Homoclinic saddle to saddle-focus transitions in 4D systems

Manu Kalia
M.Sc. Thesis
July 2017

Acknowledgements

This thesis is a culmination of my studies towards achieving a Master of Science degree in Applied Mathematics, which has seen many ups and downs, much like the sinusoidal scalar map presented in the work ahead. From leaving India for the first time and not knowing about linearising ODEs, to writing a master thesis on a new bifurcation, I look back on these two years with a smile.

The smile is due to the people and institutions that pushed me to where I am today. I'd like to thank Stefano for being a great *amico*, Xiaoming for looking through my accent and noticing how much we had in common, Ingrid and Maurice for making me feel at home, Michael for his inspiring work ethic, Milaisa for her laughter, Sietske for pointing out the good things in life, Erwin for his positivity, Niek for being inspirational and insightful at work, and the 'gang' that came in last September and February for making me feel a part of this world, and not just India.

The will to continue pursuing despite everything is mostly due to my supervisors Hil and Yuri, their enthusiasm and concern for the project instilled a lot of confidence in me. In the past two years I have gained a lot of insight into bifurcation theory (and the academic way of life) through them. They are a big part of my motivation to continue in this field. I thank them for all their guidance and am glad to remain a part of the AA chair for the coming academic year.

I would like to thank Pragya for her support and for always being there, she has been through all the ups and downs I mentioned earlier, with me. I look forward to scaling new heights by her side.

Finally, I dedicate this work to Saugata sir, my parents, my brother and my grandparents back in India. Thanks for letting me fly, crash and fly again!

Contents

Chapter 1

Introduction

बहने दो!

We introduce this Thesis by going through the significant terms used in the title: Homoclinic, saddle to saddle-focus transitions and 4D systems. We then lay down a research statement and summarise the work done.

1.1 Homoclinic orbits

If we consider the flow generated by

$$\dot{x} = \frac{dx}{dt} = f(x, \alpha), \ x \in \mathbb{R}^n, \ \alpha \in \mathbb{R}^m, \tag{1.1}$$

where f is smooth, then we can speak about its *phase portrait* near *invariant* sets for fixed parameter values. The invariance here means that solutions $x(t)$ starting from points on such a set would remain in the set $\forall t \in \mathbb{R}$. The simplest example of such a set is an *equilibrium* x_0 where $f(x_0, \alpha) = 0$ for some $\alpha = \alpha_0$.

In this Thesis we are mostly concerned with a specific kind of invariant set, namely *homoclinic orbits*. The corresponding solutions $x(t)$ have the property

$$\lim_{t \to \pm\infty} x(t) = x_0, \tag{1.2}$$

where x_0 is an equilibrium at some parameter value $\alpha = \alpha_0$. Homoclinic orbits to *hyperbolic* equilibria, whose eigenvalues λ_i are such that $Re(\lambda_i) \neq 0$, $\forall i$, are of specific interest, as they are *structurally unstable*.

When there exists a homoclinic orbit Γ_0 to a hyperbolic equilibrium x_0, upon perturbing the system by changing one of the parameters $\alpha_i, i = 1, 2, ..., m$, this homoclinic orbit generically disappears. There is then a topological nonequivalence of the local phase portrait upon changing parameters. This is called a *bifurcation*. As there is just one parameter which controls the onset of the bifurcation, it is said to have *codimension* 1.

Codimension 1 homoclinic bifurcations

For n-dimensional systems, in most cases the analysis of homoclinic bifurcations is restricted to that on the homoclinic center manifold, a k-dimensional invariant manifold such that the tangent space of this manifold at the equilibrium is spanned by eigenvectors corresponding to *leading* eigenvalues, given that certain *genericity* conditions are satisfied. Here k is the number of *leading* eigenvalues of x_0. Leading eigenvalues are the union of the stable eigenvalues with largest real part, and the unstable eigenvalues with smallest real part.

1
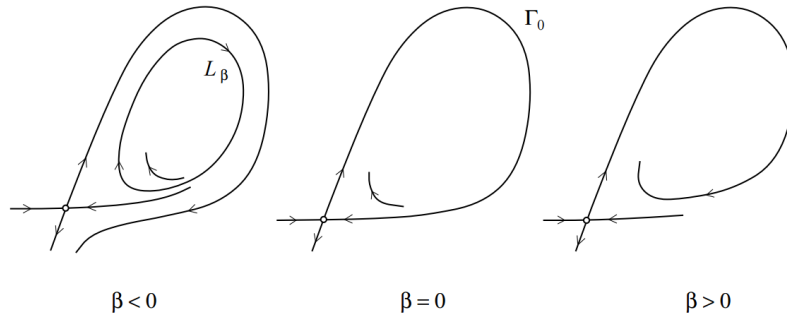
Figure 1.1: The homoclinic bifurcation in the saddle case in the plane. We see the appearance of a periodic orbit in the case where the bifurcation parameter $\beta < 0$.
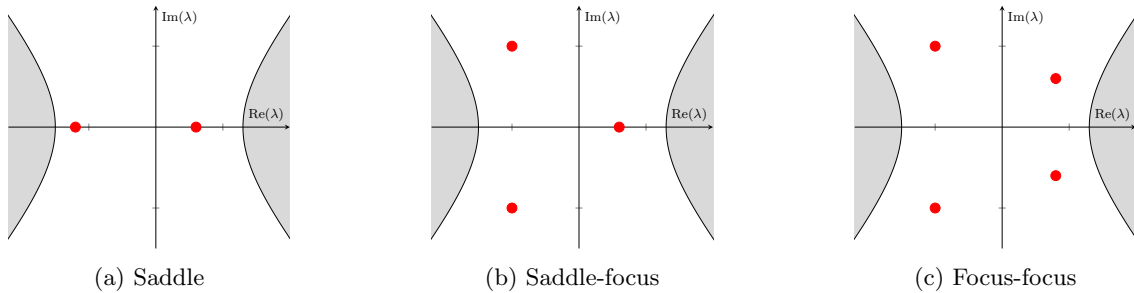
Figure 1.2: Configurations of leading eigenvalues λ (red). Gray area denotes non-leading eigenvalues.

For different configurations of the leading eigenvalues, the nature of these bifurcations is different. In Figure 1.2, we see three such configurations for which we have a detailed understanding of the bifurcations occurring close to the critical saddle and the homoclinic orbit.

For example in the saddle case, a single periodic orbit appears, see Figure 1.1 for a planar illustration. However, in the saddle-focus case, infinitely many periodic orbits can exist. This happens when the *saddle quantity* σ_0, defined by the sum of real parts of the leading unstable and stable eigenvalues, is positive. Note that in the saddle-focus case, we could assume that the leading unstable eigenvalue is complex by applying time-reversal if necessary.

1.2   Saddle to saddle-focus transitions

In this section we discuss two types of transitions from saddle to saddle-focus case. One is the standard Belyakov case [5] and the other is a newly observed transition whose analysis is done in the Thesis.

Standard saddle to saddle-focus transition: Belyakov bifurcation

Belyakov [5] and Kuznetsov et al. [13] analysed the interesting case where there is a transition from saddle to saddle-focus upon changing parameters, along a two-parameter curve of homoclinic orbits. This transition corresponds to a codimension 2 situation. Here, for $\sigma_0 > 0$ the bifurcation diagram is complex, see Figure 1.4. This is the standard, well-known saddle to saddle-focus transition.

The eigenvalue configurations are shown in Figure 1.3. Here the pair of leading complex eigenvalues approach the real axis and split into two distinct real eigenvalues. At the transition there exists a double real eigenvalue.

(a) $\alpha < 0$ (b) $\alpha = 0$ (c) $\alpha > 0$
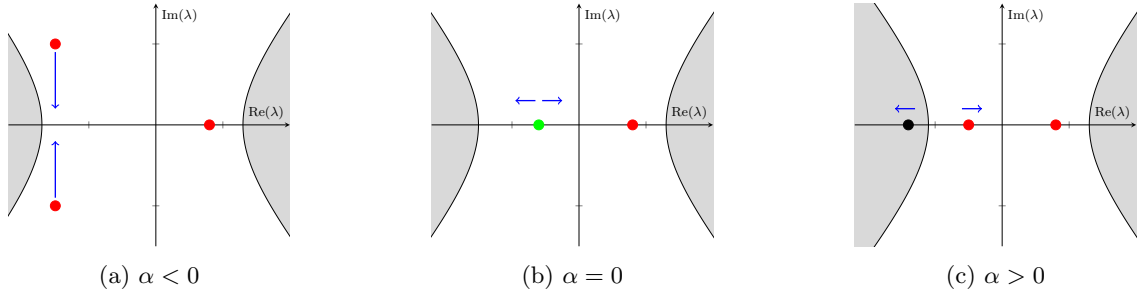
Figure 1.3: Eigenvalue (λ) configurations of the Belyakov transition along a curve of homoclinic orbits; α is the parameter along the homoclinic curve and the bifurcation occurs at $\alpha = 0$. Arrows point in the direction of generic movement of eigenvalues. The green marker indicates a double real eigenvalue. The gray area denotes non-leading eigenvalues, leading eigenvalues are marked red and non-leading eigenvalues are marked black.

In [4],[5],[13] a description of the bifurcations close to the transition and the homoclinic connection has been presented. We briefly go through some of the results here. The main observations are:

(**B.1**) There exists an infinite set of *period doubling* (PD) and *limit point* (LP) curves close to the transition and the corresponding homoclinic connection.

(**B.2**) These curves have the same structure and accumulate onto the curve of primary homoclinic orbits.

(**B.3**) There exists an infinite set of *secondary homoclinic* curves, close to the transition and the corresponding *primary* homoclinic connection. 'Secondary' refers to the homoclinic orbit making one additional global passage before returning to the saddle.
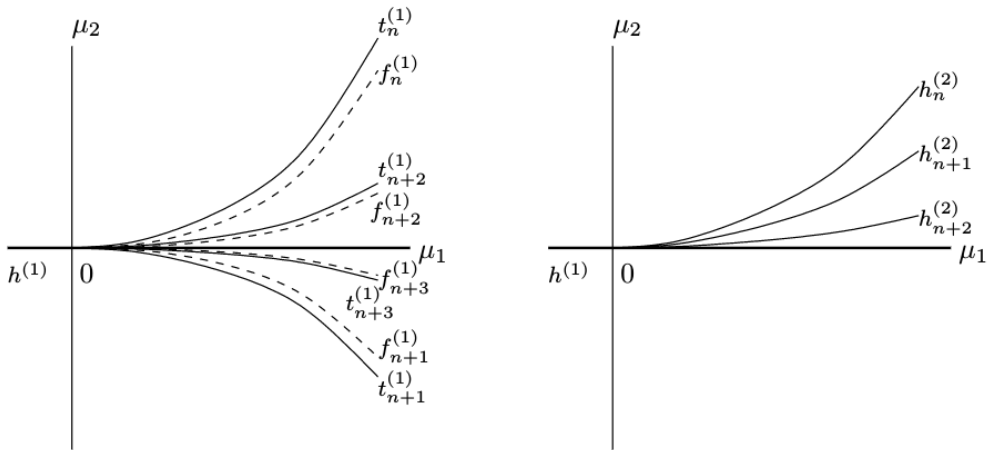
Figure 1.4: Bifurcations sets close to the Belyakov bifurcation (at 0). Here $\{t_n^{(1)}\}$ refers to the set of primary limit point curves, $\{f_n^{(1)}\}$ refers to the set of primary period doubling curves and $\{h_n^{(2)}\}$ refers to the set of secondary homoclinic curves. The parameters μ_1 and μ_2 control the eigenvalue configurations and the appearance of the homoclinic orbit respectively. Figure taken from [13].

In order to analyse the Belyakov transition, a two-parameter model return map was constructed on a cross section close to the saddle. The two parameters in this case are μ_1 and μ_2, which control the transition and the existence of the primary homoclinic connection, respectively. For μ_1 we have three cases:

- $\mu_1 < 0$: The stable leading eigenvalues are real and simple.

- $\mu_1 = 0$: We are at the transition. Here stable leading eigenvalue is a double real.

- $\mu_1 > 0$: The stable leading eigenvalues are complex.

The primary homoclinic curve exists only when $\mu_2 = 0$.

In Figure 1.4 the results can be seen. The plots show bifurcation diagrams of the model map. These are meant to give a description of the bifurcations expected close to the transition. In [13], these results are confirmed by observations of the Belyakov bifurcation in a system of ODEs.

(a) $\alpha < 0$ (b) $\alpha = 0$ (c) $\alpha > 0$
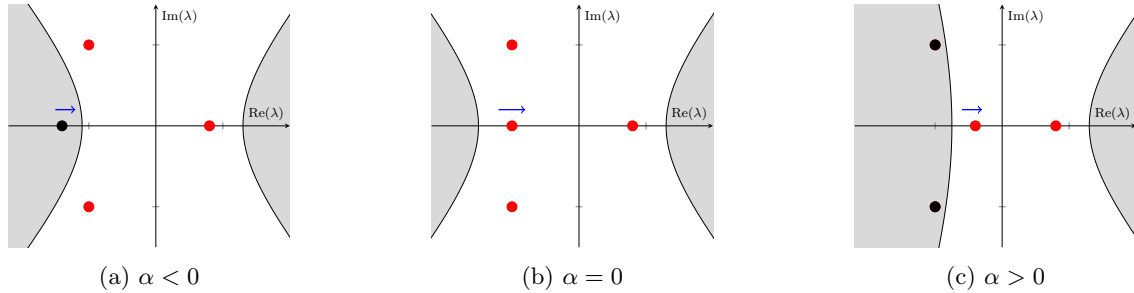
Figure 1.5: Eigenvalue (λ) configurations of the saddle to saddle-focus transition as observed in Meijer and Coombes [14]; the scalar bifurcation parameter along the curve is α. Arrows point in the direction of generic movement of eigenvalues. There is a codimension 2 situation at $\alpha = 0$, when the leading stable eigenspace becomes 3-dimensional. The gray area denotes non-leading eigenvalues, leading eigenvalues are marked red and non-leading eigenvalues are marked black.

A new saddle to saddle-focus transition in 4D systems

In Meijer and Coombes [14], an interesting transition is observed. It involves a 4-dimensional system of ODEs arising from a travelling wave study of a neural field model. In this system we have one or three equilibria, u_{low}, u_{mid} and u_{high}. At a particular parameter value, the hyperbolic equilibrium u_{low} possesses a homoclinic orbit. Along the two-parameter curve of homoclinic orbits we see that there is a saddle to saddle-focus transition, giving rise to a codimension 2 situation, which is different from the standard Belyakov case, see Figure 1.5.

Here the real eigenvalue exchanges its position with the pair of complex eigenvalues, giving rise to a situation where the stable leading eigenspace is three dimensional. Thus at the transition there exist two complex eigenvalues and one real eigenvalue with the same real part. All leading eigenvalues are simple.

In Figure 1.6, real parts of eigenvalues along the homoclinic curve mentioned above are plotted against one of the parameters β. In **(A)** we see the new transition, where the pair of complex stable eigenvalues cross the stable real eigenvalue transversally, giving rise to a codimension 2 situation. The leading stable eigenspace at this transition is three dimensional. However, in [14] the transition is observed only in the *tame* case ($\sigma_0 < 0$).

1.3   Research statement

The new transition mentioned in the previous section, observed in Meijer and Coombes [14] in the tame case is the motivation for this Thesis. We would like to understand phase portraits close to the critical saddle and the homoclinic orbit at the tame and wild transition, for small perturbations of the flow.

What is the goal of this work?
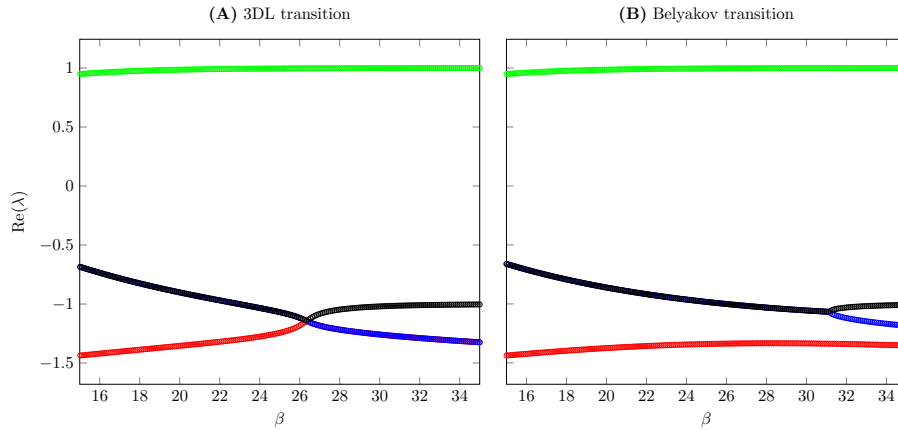
Figure 1.6: Plot of the real part of the eigenvalues vs. a parameter β along a curve of homoclinic orbits, as obtained from the ODE system in [14]. In **(A)**, we see that the branches corresponding to stable complex and real eigenvalues (red and black curves) cross transversally. At the crossing point, the stable leading eigenspace is 3-dimensional. In **(B)**, we see the Belyakov transition where a pair of complex eigenvalues (black curve) split into two distinct real eigenvalues (black and blue curves). The leading stable eigenspace at the Belyakov bifurcation is 2-dimensional.

We aim to give a detailed description of bifurcations occurring in a small fixed neighbourhood of $U = \Gamma_0 \cup x_0$ where Γ_0 is the homoclinic orbit and x_0 is the saddle, at the transition, i.e. when the stable (unstable) leading eigenspace is three dimensional.

How will this goal be met?

- In order to observe the phase portrait of the transition under small, two-parameter perturbations, we consider a 4-dimensional system satisfying the transition conditions and some *genericity* conditions. We then introduce cross-sections, close to the critical saddle and transversal to the flow. By looking at orbits departing and returning to the cross-sections, we obtain a model map on the cross-section.

- Fixed points of this map correspond to periodic orbits, and bifurcations of these fixed points correspond to bifurcations of periodic orbits. Thus, analysis of this map gives us an understanding of bifurcations of periodic orbits close by.

- We also derive a model map for secondary homoclinic orbits with the above technique and analyse the same.

Note: For the remainder of the Thesis we will be dealing with 4-dimensional ODE systems only. By applying time-reversal when necessary, we can assume without loss of generality for the remainder of the Thesis, that at the bifurcation, the leading stable eigenspace is 3-dimensional and the leading unstable eigenspace is 1-dimensional. From here on we refer to this transition point, as the **3DL (3-dimensional leading) transition**, for convenience. The corresponding bifurcation and saddle are referenced in the same way too.

1.4 Organisation and summary

The Thesis begins with an introduction to homoclinic orbits in **Chapter 2**. Then we briefly outline theorems describing bifurcations of hyperbolic homoclinic orbits in the saddle and saddle-focus cases. We also discuss center manifold theorems, which describe how the understanding of these bifurcations in higher dimensional systems can be reduced to looking at generic two, three or four dimensional systems.

(A) Scalar model map

(B) Spring area in scalar map

(C) Secondary homoclinics

(D): 3D model map
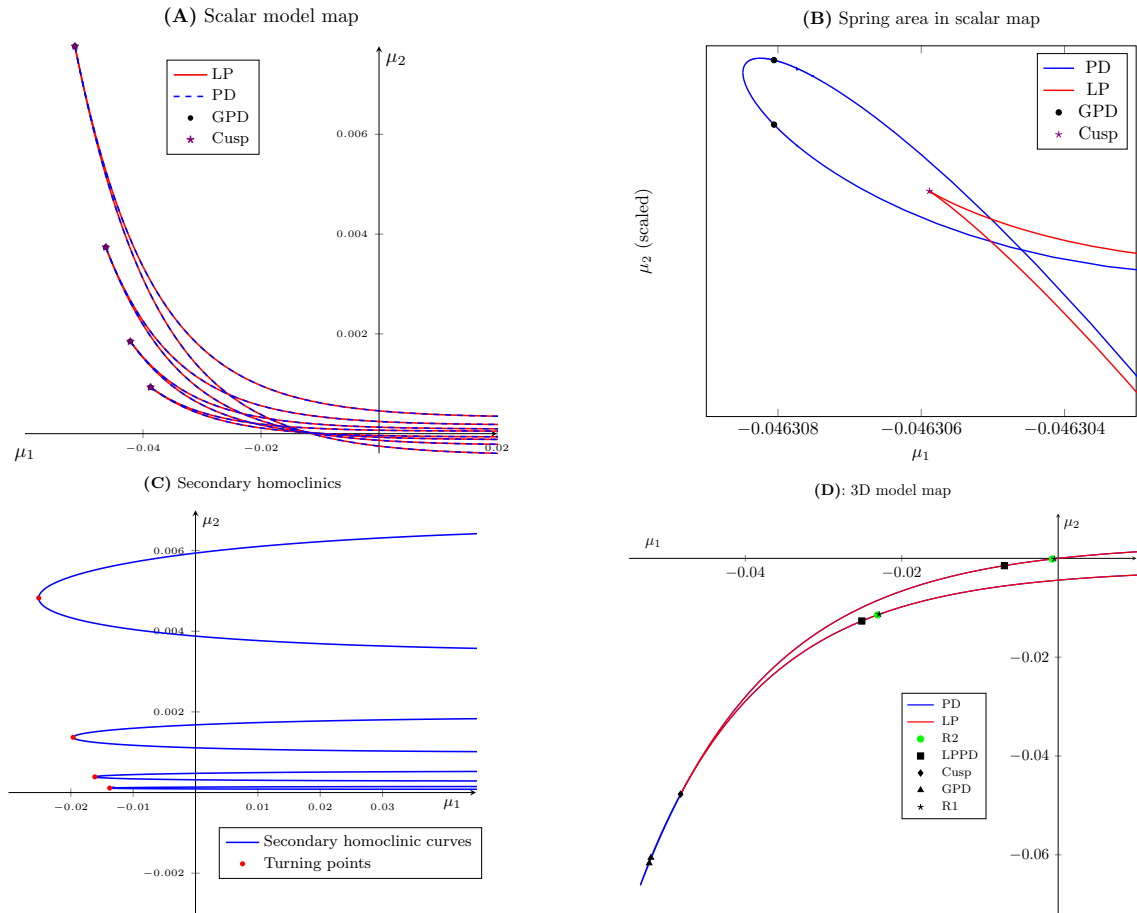
Figure 1.7: Summary of bifurcations occurring close to the 3DL transition. μ_1 controls the eigen-value configuration. For $\mu_1 < 0$ we have the saddle case, for $\mu_1 = 0$ we have the 3DL saddle and for $\mu_1 > 0$ we have the saddle-focus case. The primary homoclinic connection exists only when $\mu_2 = 0$. In **(A)** PD and LP *horns* of the *scalar model map* are plotted. In **(B)** the *spring area* at the tip of the horn is shown. In **(C)** secondary homoclinic 'parabolas' and their corresponding turning points are plotted. In **(D)** a single PD/LP horn of the *3D model map* is plotted, along with several codimension 2 points found along it.

In **Chapter 3**, we introduce Poincaré maps close to the 3DL saddle in a general 4-dimensional system with a homoclinic connection. A three-dimensional model return map is formulated in the same spirit as for the Belyakov transition, which can be further reduced to a scalar map. The scalar map obtained is different from other model maps (saddle, saddle-focus and Belyakov cases).

In **Chapter 4** we look into 4 topics:

1. We analyse the scalar map for its fixed points, which gives information about bifurcations of cycles occurring close to the critical saddle and its homoclinic orbit. Here we obtain an infinite sequence of PD and LP curves accumulating onto the primary homoclinic curve. However, the nature of accumulation is very different from that in the Belyakov case, e.g. Figure 1.7. The PD/LP curves form *horns*, which are characterised by codimension 2 bifurcation points and subtle structures (called *spring (saddle) areas*, see [15]) close to such points.

2. From the scalar map, we derive expressions describing the asymptotic behaviour of codimension 1 bifurcation curves. The asymptotics agree with the results obtained from numerical continuation and provide a deeper understanding of the bifurcation sets.

3. We derive and analyse a scalar model map for secondary homoclinic orbits occurring close

to the bifurcation. In this case too, there exists an infinite set of bifurcation curves corresponding to secondary homoclinic orbits, that accumulate onto the primary homoclinic curve. These curves also have a structure that is different from the Belyakov case. Each curve forms a horizontal parabola and possesses a turning point. The sequence formed by these points approaches the 3DL bifurcation point asymptotically.

4. We provide analytical expressions describing the asymptotic behaviour of the set of secondary homoclinic curves. The results agree well with those obtained from numerical continuation.

In **Chapter 5**, the full 3-dimensional model map is analysed numerically. The structure of PD/LP curves is the same as that in the scalar case. The spring area is observed here too. The difference from the scalar case is that more cascades of codimension 2 points are observed, such as *fold-flip* and *strong resonances*. The 1:1 and 1:2 resonance points are connected via a primary *Neimark-Sacker* (NS) curve.

We note that the spring area in the 3D case does not imply that the same phenomenon exists in the scalar case or vice-versa. It must also be noted here that the model map for secondary homoclinic curves is scalar and no higher dimensional map needs to be derived from the considered model flow.

We end the thesis with a summary in **Chapter 6**, where we also discuss how the results differ from the Belyakov case. We briefly note some ideas that can be explored in future, to obtain better knowledge of bifurcation sets near the 3DL transition.

Chapter 2

Homoclinic bifurcations and transitions

2.1 Bifurcations in continuous and discrete-time dynamical systems

Consider a vector field,

$$\dot{x} = f(x, \alpha), \quad x = (x_1, x_2, ..., x_n) \in \mathbb{R}^n, \quad \alpha \in \mathbb{R}^m. \tag{2.1}$$

Then x_0 is an *equilibrium* at $\alpha = \alpha_0$ for this system if $f(x_0, \alpha_0) = 0$. Let $J = f_x(x_0, \alpha_0)$ be the matrix of the linearisation around this equilibrium at α_0. We introduce the notion of *hyperbolic* equilibria.

Definition 2.1.1. An equilibrium x_0 of (2.1) is said to be *hyperbolic* if none of the eigenvalues of J have zero real part.

We can define the same concept for *fixed points* of iterated maps. Consider

$$x \mapsto f(x, \alpha), \quad x = (x_1, x_2, ..., x_n) \in \mathbb{R}^n, \quad \alpha \in \mathbb{R}^m, \tag{2.2}$$

at $\alpha = \alpha_0$. Then x_0 is a fixed point of this system if $f(x_0, \alpha_0) = x_0$. Let $J = f_x(x_0, \alpha)$ be the Jacobian matrix of (2.2) evaluated at the fixed point. The *multipliers* of this map at x_0 are defined as the eigenvalues of J.

Definition 2.1.2. A fixed point x_0 of (2.2) is said to be *hyperbolic* if none of the multipliers μ of x_0 are such that $|\mu| = 1$.

Hyperbolic equilibria and fixed points are interesting because of their structural stability. It is then possible to point out when the phase portraits around these equilibria (or fixed points) differ topologically, based on the eigenvalues (or multipliers) of the Jacobian evaluated at the equilibria (or fixed points). To make this argument more precise, we discuss the results on *topological equivalence* in brief.

Topological equivalence

Two vector fields are said to be *topologically equivalent* if there exists a homeomorphism (a continuous invertible map with a continuous inverse) mapping orbits of one vector field onto those of the other. The same definition holds for iterated maps.

We have the following result regarding topological equivalence local to the equilibrium x_0 of (2.1):

Theorem 2.1.1. *Let x_0 and y_0 be two hyperbolic equilibria of system (2.1). Then the vector fields around these two equilibria are locally topologically equivalent if the linearisations around these two equilibria have the same number of positive and negative eigenvalues.*

Equivalently, for an equilibrium x_0 at α_0 of (2.1), the phase portrait around the equilibrium x_1 obtained after a small change of parameter $\alpha_0 \mapsto \alpha_0 + \epsilon$, for small $\|\epsilon\|$, is locally topologically equivalent to the phase portrait around x_0 if the linearisations $J_1 = f_x(x_0, \alpha_0)$ and $J_2 = f_x(x_1, \alpha_0 + \epsilon)$ have the same number of positive and negative eigenvalues.

We have a similar result for fixed points x_0 of (2.2):

Theorem 2.1.2. *Let x_0 and y_0 be two hyperbolic fixed points of system* (2.2). *Then the phase portraits around these two fixed points are locally topologically equivalent if the linearisation around these two fixed points have the same number of multipliers μ satisfying*

1. *$|\mu| < 1$ and $|\mu| > 1$.*

2. *The signs of the products of all the multipliers with $|\mu| < 1$ and $|\mu| > 1$ are the same for both fixed points.*

The loss of local topological equivalence between two equilibria/fixed points of the same system obtained upon small change of parameters is called a *bifurcation*. From the theorems on local topological equivalence, we can already expect that a bifurcation must be associated with a change in the number of positive and negative eigenvalues in case of ODEs. In the case of maps, we expect a bifurcation to occur when the number of multipliers with modulus greater than 1 (or smaller than 1) changes.

We present a result here describing the *structural stability* of hyperbolic equilibria.

Theorem 2.1.3. *A hyperbolic equilibrium is structurally stable under smooth perturbations.*

This means that under sufficiently small perturbations to the vector field in terms of small changes in parameters, the corresponding equilibria remain hyperbolic. This would imply that a bifurcation of an equilibrium is associated with the loss of hyperbolicity. The result is analogous in the case of fixed points.

The simplest bifurcation is observed in the scalar (one-dimensional) vector field

$$\dot{x} = f(x, \alpha), \quad x, \alpha \in \mathbb{R}.$$

As there is only one eigenvalue $\lambda = f_x(x_0, \alpha_0)$, the equilibrium would become nonhyperbolic if $\lambda = f_x(x_0, \alpha_0) = 0$. This bifurcation is called the *fold bifurcation*, and occurs for vector fields of dimension $n \geq 1$. In planar (2-dimensional) vector fields, as there are two eigenvalues, the loss of hyperbolicity is associated with a pair of complex eigenvalues crossing the imaginary axis or a real eigenvalue becoming 0, upon varying parameters. The former is called the *Hopf bifurcation* and the latter is the fold bifurcation.

2.1.1   Topological normal forms

To explain how phase portraits change (with respect to topological equivalence), we introduce the concept of *topological normal forms*.

Consider

$$\dot{x} = f(x, \alpha), \quad x \in \mathbb{R}^n, \ \alpha \in \mathbb{R}^m, \tag{2.3}$$

with equilibrium $x_0 = 0$ which undergoes a bifurcation at $\alpha = 0$. Let there be k conditions for the bifurcation to occur. This value k is called the *codimension* of the bifurcation. Let us also consider

$$\dot{y} = g(y, \beta, \sigma), \quad x \in \mathbb{R}^n, \ \beta \in \mathbb{R}^k \text{ and } \sigma \in \mathbb{R}^l, \tag{2.4}$$

where g is polynomial in y. At $\beta = 0$ we have an equilibrium at $y = 0$ which undergoes a bifurcation and the parameter k is the codimension from before. The coefficients of the polynomial $g(y)$ constitute σ. They usually assume a fixed number of integral values, as we shall see in an example, ahead.

Definition 2.1.3. System (2.4) is said to be a *topological normal form* for the corresponding bifurcation if any system (2.3) satisfying certain genericity conditions is locally topologically equivalent to system (2.4) near the equilibrium $x_0 = 0$ for some values of the coefficients σ.

The *genericity* conditions are inequalities that allow the parameters to 'unfold' the singularity (the equilibrium at the bifurcation) in a general fashion and guarantee nondegeneracy.
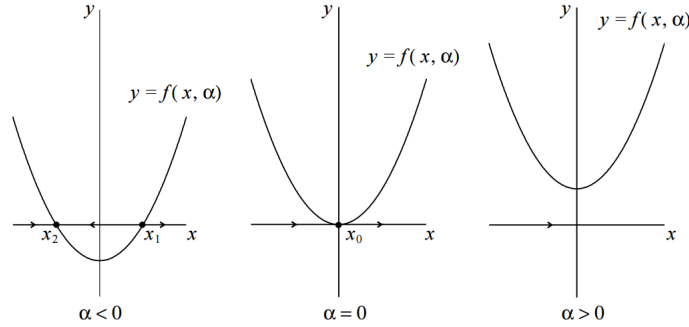
Figure 2.1: Fold bifurcation of an equilibrium of a scalar ODE $\dot{x} = f(x, \alpha)$. We see that as we change α (the bifurcation parameter in the normal form) from negative to positive, two equilibria collide and disappear.

Example: Normal form of fold bifurcation

To illustrate, we consider the simple *fold* bifurcation which was introduced earlier. The fold bifurcation in a scalar system is associated with an eigenvalue of any of its equilibria becoming 0.

Let us consider that the ODE

$$\dot{x} = f(x, \alpha), \quad x \in \mathbb{R}, \ \alpha \in \mathbb{R}, \tag{2.5}$$

with f smooth, has an equilibrium $x_0 = 0$ which undergoes a fold bifurcation at $\alpha = 0$. The bifurcation condition is

$$f_x(0, 0) = 0.$$

Via smooth coordinate transformations and introducing a new parameter it can be shown that (2.5) is generically smoothly equivalent to the ODE

$$\dot{y} = \beta + y^2 + O(y^3), \tag{2.6}$$

where β is a new scalar parameter and $s = \pm 1$, see [12]. In order to transform (2.5), Implicit Function Theorem is used multiple times to eliminate the linear term and obtain the constant s. There are *genericity* conditions for the fold bifurcation. In order to transform (2.5) to (2.6), we need the following (generic) assumptions:

(F.1) $f_{xx}(0, 0) \neq 0$.

(F.2) $f_\alpha(0, 0) \neq 0$.

Finally, it can also be shown [12] that (2.6) is locally topologically equivalent near the origin to the system

$$\dot{y} = \beta + y^2. \tag{2.7}$$

Therefore (2.7) is a topological normal form for the fold bifurcation, near the corresponding equilibrium. Now that we have the normal form, we can analyse this system to understand the local phase portrait at the bifurcation point for small perturbations.

We see that, for $\beta < 0$, there exist two equilibria $y^{\pm} = \pm\sqrt{\beta}$. For $\beta > 0$, there exist no equilibria. At the equilibrium $y = 0$ for $\beta = 0$, we see that the corresponding eigenvalue is zero. This is the fold bifurcation. Thus, upon changing $\beta = -\epsilon$ to $\beta = \epsilon$ for ϵ sufficiently small and positive, the equilibria $y^{\pm}$ collide and disappear.

Therefore for any system (2.5) where a fold bifurcation occurs, two equilibria collide and disappear upon perturbing the vector field, nearby. Such a system must also obey the genericity conditions **F.1-2**.

It must be noted that such normal forms do not exist for all bifurcations and in many cases, the truncated normal form does not provide a complete understanding of the local phase portrait. However, their existence has a universal meaning, since any generic system satisfying the bifurcation conditions would have the local phase portrait around the singularity, as described by the corresponding normal form.

2.1.2 Bifurcations of equilibria in $n-$ dimensional systems

The fold bifurcation may occur in an $n-$dimensional system. If we consider the system

$$\dot{x} = f(x, \alpha), \quad x = (x_1, x_2, ..., x_n) \in \mathbb{R}^n, \quad \alpha \in \mathbb{R}, \tag{2.8}$$

then a fold bifurcation occurs at equilibrium $x = 0$ for parameter $\alpha = 0$ if any one of its eigenvalues become zero.

Here too, two equilibria collide and disappear, in the same way as in the scalar $(n = 1)$ case. This is explained by the reduction of $n-$dimensional systems to $1-$dimensional *center manifolds*. These manifolds are invariant, attracting and have the property that the dynamics of structural instability of the $n-$dimensional system can be determined by the restriction of the flow on the $1-$dimensional manifold.

In general the center manifold is $k-$dimensional, were k is the number of eigenvalues of the singularity lying on the imaginary axis.

Let T^c be the eigenspace defined by the corresponding eigenvectors of such eigenvalues. We have the following result.

Theorem 2.1.4. (Center Manifold Theorem) *There is a locally defined smooth $k-$dimensional invariant manifold $W^c_{loc}(0)$ of (2.8) that is tangent to T^c at $x = 0$. Moreover, there is a neighbourhood U of $x_0 = 0$, such that if the orbit $x(t) \in U$ for $t \geq 0$, then $x(t) \to W^c_{loc}(0)$ for $t \to \infty$. The manifold $W^c_{loc}(0)$ is called the center manifold.*

The results also hold when time is reversed. It is possible to change basis and collect *noncritical* and *critical* states as follows

$$\begin{cases} \dot{u} = Au + f(u, v), \\ \dot{v} = Bv + g(u, v), \end{cases} \tag{2.9}$$

where $A \in \mathbb{R}^k \times \mathbb{R}^k$ is such that all its eigenvalues lie on the imaginary axis. The matrix $B \in \mathbb{R}^{n-k} \times \mathbb{R}^{n-k}$ is such that none of its eigenvalues lie on the imaginary axis. The functions f and g are at least quadratic in Taylor expansions. From the theorem above, we are guaranteed a center manifold. This manifold W^c is the of the form

$$W^c = \{(u, v) \ : \ v = V(u)\},$$

such that $V(u) = O(\|u\|^2)$ due to the tangent property. Then we have the following *reduction principle*.

Theorem 2.1.5. (2.9) *is locally topologically equivalent near the origin to the system*

$$\begin{cases} \dot{u} = & Au + f(u, V(u)), \\ \dot{v} = & Bv. \end{cases} \tag{2.10}$$

For non-unique center manifolds, all resulting systems (2.10) *are locally smoothly equivalent, which is to say that there exists a homeomorphism mapping orbits of* (2.9) *to* (2.10) *while preserving the direction of time.*

It is clear that (2.10) is uncoupled. As the eigenvalues of B are away from the imaginary axis, the dynamics of v are structurally stable and the structural instability of (2.8) is essentially determined by the dynamics of u in (2.10). This means that in order to understand the nature of the local phase portrait close to the bifurcation under small perturbations, the restriction of the flow on the center manifold gives complete information, thereby simplifying the problem by reducing dimensionality and allowing the bifurcation to exist in the same way for higher dimensional systems, irrespective of the dimension.

So far, we fixed the parameter α. It can also be shown that there exist parameter dependent center manifolds. Let us consider

$$\left\{ \begin{array}{l} \dot{\alpha} = 0, \\ \dot{x} = f(x, \alpha). \end{array} \right.$$

where f is from (2.8). The system has a nonhyperbolic equilibrium at $(\alpha, x) = (0, 0)$. From Theorem 2.1.4, there exists a center manifold W^c. The set $\Pi_{\alpha_0} = \{(\alpha, x) : \alpha = \alpha_0\}$ is invariant with respect to the above flow. Therefore we can consider the invariant manifolds

$$W^c_\alpha = W^c \cap \Pi_\alpha,$$

which *foliate* the center manifold W^c. Now for each small $|\alpha|$, we can restrict the flow (2.8) to the invariant manifold W^c_α to obtain the system

$$\dot{u} = \Phi(u, \alpha). \tag{2.11}$$

We have the following result

Theorem 2.1.6. *System* (2.8) *is locally topologically equivalent to the system*

$$\left\{ \begin{array}{l} \dot{u} = \Phi(u, \alpha), \\ \dot{v} = -v, \\ \dot{w} = w, \end{array} \right.$$

where $u \in \mathbb{R}^k, v \in \mathbb{R}^{n^-}$ *and* $w \in \mathbb{R}^{n^+}$. *Here* $n^+(n^-)$ *is the number of eigenvalues with positive (negative) real part. Moreover,* (2.11) *can be replaced by any locally topologically equivalent system.*

Thus all essential events near the bifurcation parameter value occur on W^c_α and can be determined by the $k-$dimensional system (2.11).

Example: Fold bifurcation in n-dimensional systems

Let us consider the fold bifurcation in an $n-$dimensional system. It is characterized by one of the eigenvalues becoming zero. However, Theorem 2.1.4 and Theorem 2.1.6 guarantee the existence of a parameter dependent local invariant manifold W^c_α near the bifurcation. This manifold is one-dimensional and we can determine the nature of the phase portraits by restricting the flow on this manifold. The restriction is topologically equivalent to the normal form (2.7), which proves that the fold bifurcation would have the same behaviour in the phase portrait, irrespective of the value of n. Thus topological normal forms can explain bifurcations in generic higher dimensional systems.
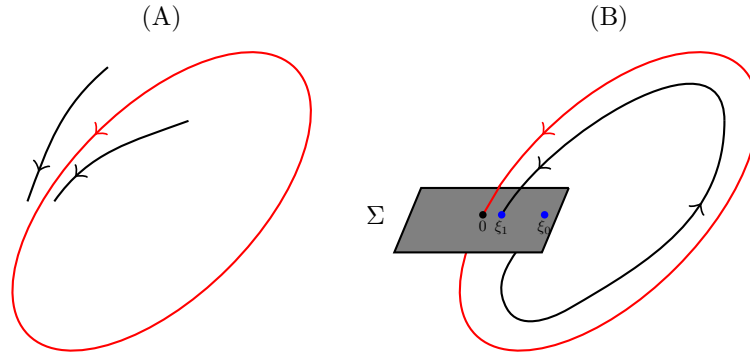
Figure 2.2: An impression of a periodic orbit. In **(A)**, we see a *stable* periodic orbit. In some tubular ϵ−neighborhood around this periodic orbit, all orbits converge onto the cycle. In **(B)**, we see how Poincaré maps are used to analyze the behavior of periodic orbits. The red curve is a cycle, passing through the cross-section Σ at $\xi = 0$. Thus $\xi = 0$ is a fixed point of the return map from Σ to itself. The black orbit corresponds to a non-periodic solution. It first meets Σ at $\xi = \xi_0$. However, when the orbit returns back, it meets Σ at $\xi = \xi_1 \neq \xi_0$. Thus the non-periodic orbit corresponds to an ordinary point (not a fixed point) of the return map defined on Σ.

2.2 Periodic orbits and global bifurcations

Let us consider (2.1) again, i.e.

$$\dot{x} = f(x, \alpha), \quad x = (x_1, x_2, ..., x_n) \in \mathbb{R}^n, \quad \alpha \in \mathbb{R}^m.$$

Then, a solution $x(t)$ of the above system is said to be a periodic if

$$x(t + T) = x(t), \; \forall t, \tag{2.12}$$

for some $T > 0$. The minimal T is called the *period* of the periodic solution. Orbits corresponding to periodic solutions are called periodic and are also referred to as *(limit) cycles*. A stable periodic orbit can be seen in Figure 2.2. Just like fixed points (equilibria) of iterated maps (ODEs), periodic orbits also undergo bifurcations. The simplest bifurcation is the fold bifurcation for cycles, which involves two cycles colliding and disappearing (Figure 2.3).

Understanding global bifurcations with Poincaré maps

Interestingly, the analysis of cycles can be reduced to that of fixed points, for which we already have a catalogue of results [12]. This is done by the *Poincaré map* technique, where we consider a hyperplane in the neighbourhood of a point on the cycle, such that the hyperplane is transversal to the flow. An example of this cross section Σ an be seen in Figure 2.2. Thus, the Poincaré map transforms the point of departure of the orbit on Σ to the point of return back to Σ. If we define a coordinate ξ on this cross section, then we can quantitatively describe the behavior of this periodic orbits upon perturbing the vector field.

For example, let Π be the Poincaré map defined on Σ with coordinate ξ, then a stable (unstable) fixed point ($\xi = 0$) corresponds to a stable (unstable) periodic orbit, see Figure 2.2. If we consider an orbit on Σ under iterations of the map Π, then a closed invariant orbit of Π would be a periodic orbit in the ODE system and aperiodic otherwise. Closed invariant orbits include fixed points and cycles with $n > 1$ elements. A cycle of the map Π with n elements would correspond to a periodic orbit in the ODE system, making n global turns. It is therefore possible to describe global dynamics of periodic orbits to an extent, with the Poincaré map technique.

This concept can then also be used to study bifurcations of periodic orbits. For example, the aforementioned fold bifurcation of cycles can be translated to the fold bifurcation for fixed points
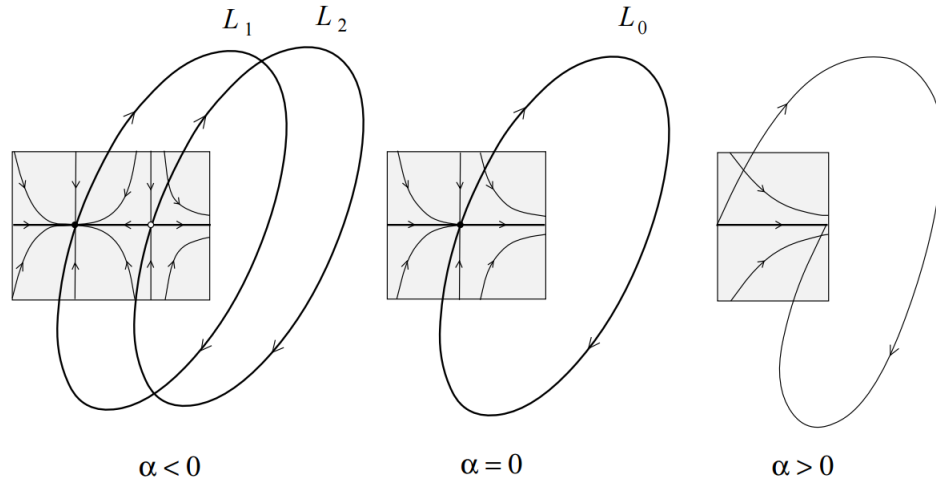
Figure 2.3: Fold bifurcation of cycles. As we change α (the bifurcation parameter in the normal form) from negative to positive, we see that two fixed points on the Poincaré cross section collide and disappear, corresponding to a fold bifurcation of fixed points.

of Π, the Poincaré map defined on Σ. For small changes in a parameter around $\xi = 0$, we see that two fixed points of Π collide and disappear. This then translates to two cycles, colliding and disappearing, see Figure 2.3.

Bifurcations of periodic orbits in higher dimensional systems

Theorem 2.1.4 is analogous in the case of fixed points. If we consider a map Π such that at $x = 0$ and $\alpha = 0$ we have a fixed point then an eigenvalue μ is a *critical* eigenvalue if $|\mu| = 1$. If k is the number of critical eigenvalues, then we are guaranteed a center manifold W^c of dimension k which is tangent to the critical eigenspace T^c at $x = 0$ [12]. Therefore the problem of structural instability of periodic orbits upon perturbing the vector field can be reduced to looking at the dynamics of the restriction of the return map $\Pi : \Sigma \mapsto \Sigma$ on the center manifold W^c for small changes in parameter values, where Σ is a hyperplane transversal to the critical periodic orbit.
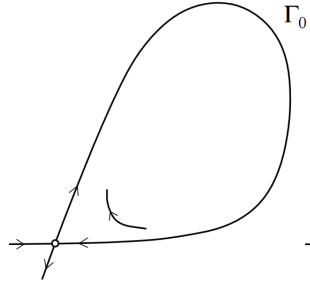
Figure 2.4: A homoclinic orbit to a saddle in the plane. Taken from [12]

2.3 Bifurcation theory and homoclinic orbits

Once again, we consider the system of ODEs

$$\dot{x} = f(x, \alpha), \quad x = (x_1, x_2, ..., x_n) \in \mathbb{R}^n, \quad \alpha \in \mathbb{R}^m. \tag{2.13}$$

A solution Γ_0 (and the corresponding orbit $\gamma_0(t)$) for the flow (2.13) is said to be homoclinic to the equilibrium x_0 if

$$\lim_{t \pm \infty} \gamma_0(t) = x_0. \tag{2.14}$$

A planar homoclinic orbit is sketched in Figure 2.4. Let

$$W^s(x_0) = \left\{ y \in \mathbb{R}^n \mid x(0) = y, \ \dot{x} = f(x, \alpha_0) \text{ and } \lim_{t \to \infty} x(t) = x_0 \right\}, \quad \text{and}$$

$$W^u(x_0) = \left\{ y \in \mathbb{R}^n \mid x(0) = y, \ \dot{x} = f(x, \alpha_0) \text{ and } \lim_{t \to -\infty} x(t) = x_0 \right\}, \tag{2.15}$$

be the stable and unstable manifolds of x_0 respectively. Therefore by definition of a homoclinic orbit,

$$\Gamma_0 \in W_u(x_0) \cap W_s(x_0).$$

Note that homoclinic orbits exist for both hyperbolic and non-hyperbolic equilibria. However, in this Thesis, we are concerned only with homoclinic orbits to hyperbolic equilibria, see Figure 2.4. These homoclinic orbits are of interest as they are structurally unstable, which means that they disappear for small perturbations of the vector field. This is then a *bifurcation* of the vector field, since the perturbed and unperturbed phase portraits are topologically non-equivalent to each other. We will now briefly outline the proof of the structural instability of orbits homoclinic to hyperbolic equilibria.

Structural stability of homoclinic orbits

Theorem 2.3.1. *Consider* (2.13). *Let there exist a homoclinic orbit* Γ_0 *to a hyperbolic equilibrium* x_0 *of the system, at* $\alpha = 0$. *Then this homoclinic orbit is structurally unstable.*

Proof. From transversality theory, we have the following statements:

> **(T.1)** Two manifolds $M, N \in \mathbb{R}^n$ intersect transversally if there exist at least n linearly independent vectors in $\mathbb{R}^n$ that are tangent to at least one of those manifolds at the point of intersection.

> **(T.2)** If the intersection of M and N is transversal, the intersection will remain transversal for small C^1 perturbations of these manifolds. If it is non-transversal, the manifolds no longer intersect upon *generic* small perturbations.

Now, we have a homoclinic orbit Γ_0 to the equilibrium x_0. As the equilibrium is hyperbolic, we have

$$n = n^+ + n^-,$$
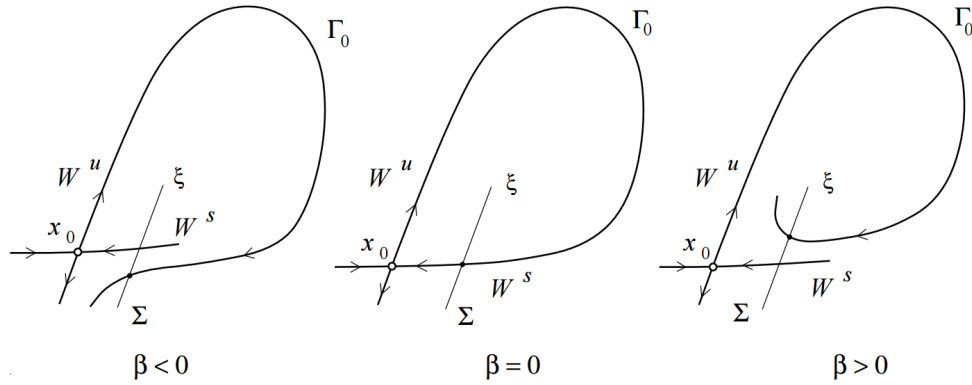
Figure 2.5: A homoclinic orbit to a hyperbolic equilibrium x_0. Σ is a cross section defined transversal to the stable manifold and ξ is the coordinate defined on it. β is the splitting function. We can observe here the structural instability of the homoclinic orbit, quantified by the splitting function β. Figure taken from [12]

(a) Saddle (2-D system)   (b) Saddle-focus (3-D system)
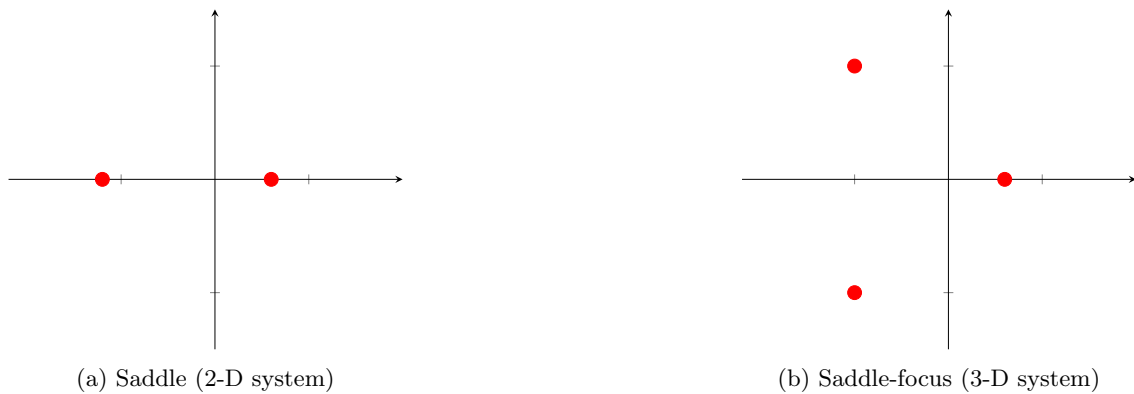
Figure 2.6: Configurations of eigenvalues in the complex space of the critical saddle which possesses a homoclinic orbit.

where n^+ is the number of eigenvalues at x_0 with positive real part. n^- is the number of eigenvalues with negative real part. The orbit $\Gamma_0 \in W_u(x_0) \cap W_s(x_0)$. As $\dim(W_u(x_0)) = n^+$ and $\dim(W_s(x_0)) = n^-$ from the Local Stable Manifold Theorem [12], the intersection will have at most $n^+ + n^- - 1 = n - 1$ linearly independent tangent vectors, implying that the intersection cannot be transversal. Hence the intersection is non-transversal and the homoclinic orbit is structurally unstable. $\square$

In Figure 2.5 we see the splitting of the homoclinic orbit. As the orbit returning along the stable manifold 'misses' the unstable manifold, we can define a cross-section transversal to the unstable manifold which quantifies the magnitude of the splitting depending on parameters. For a cross section Σ transversal to the stable manifold W^s, we define the coordinate ξ along it. The split function β is then defined by the value of ξ where the returning orbit along the unstable manifold W^u intersects the cross-section Σ. Clearly, at $\xi = 0$, the orbit returns to W^s via a non-transversal intersection between W^u and W^s and we have a homoclinic orbit.

Types of homoclinic bifurcations

So far we know that homoclinic orbits to hyperbolic equilibria are structurally unstable. As we make C^1 perturbations to the corresponding vector field, the connection breaks. The resulting phase portrait is topologically inequivalent to the previous one, and thus we have a bifurcation.
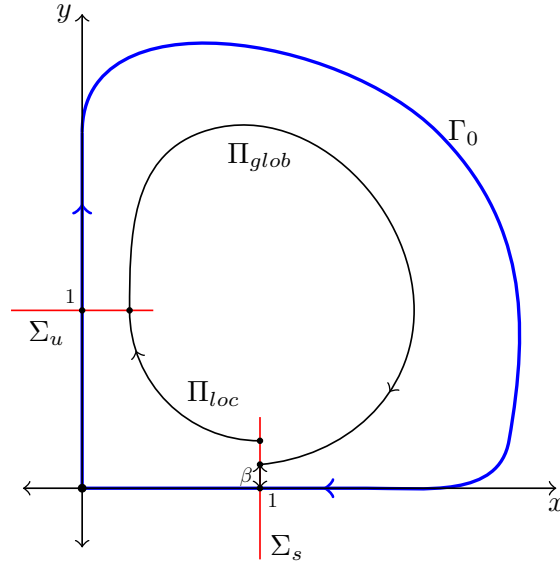
Figure 2.7: The geometric construction of cross sections for the Andronov-Leontovich Theorem (Theorem 2.3.2).

In the planar case, this is completely characterized by the Andronov-Leontovich Theorem. In the 3-dimensional case, Shil'nikov theorems explain the dynamics for different configurations of the eigenvalues.

In the forthcoming sections we discuss the nature of phase portraits for two configurations of the eigenvalues, see Figure 2.6. In the end, the Homoclinic Center Manifold Theorem describes how the results in 2 or 3-dimensional systems apply to general higher dimensional systems where a homoclinic orbit exists to a saddle equilibrium.

2.3.1   Homoclinic orbit to a saddle

An equilibrium x_0 of (2.1) is called a *saddle*, if it has at least one pair of eigenvalues such that their real parts are opposite in sign. Moreover, the leading stable eigenvalue, which is the negative eigenvalue with smallest absolute real part, must be real. In the case that the leading stable eigenvalue is complex, we call the corresponding equilibrium a *saddle-focus*.

Theorem 2.3.2. *(**Andronov-Leontovich**) Let us consider a planar system with a single parameter*

$$\dot{x} = f(x, \alpha), \ x \in \mathbb{R}^2, \alpha \in \mathbb{R}, \tag{2.16}$$

such that f is smooth and let us assume that there exists a homoclinic orbit Γ_0 to a hyperbolic equilibrium $x_0 = 0$ with eigenvalues $\lambda_1(0) < 0 < \lambda_2(0)$. We make the following assumptions for genericity:

1. *The saddle quantity $\sigma_0 = \lambda_1(0) + \lambda_2(0) \neq 0$.*

2. *$\beta'(0) \neq 0$, where $\beta(\alpha)$ is the split function dependent on the parameter α.*

Then, for sufficiently small α, there exists a neighborhood U_0 around $\Gamma_0 \cup x_0$ where a periodic orbit $P(\beta)$ bifurcates, dependent on the splitting function. The stability of $P(\beta)$ depends on the value of β and σ_0:

- *For $\beta > 0$ and $\sigma_0 < 0$ the periodic orbit is stable.*

- *For $\beta < 0$ and $\sigma_0 > 0$ the periodic orbit is unstable.*
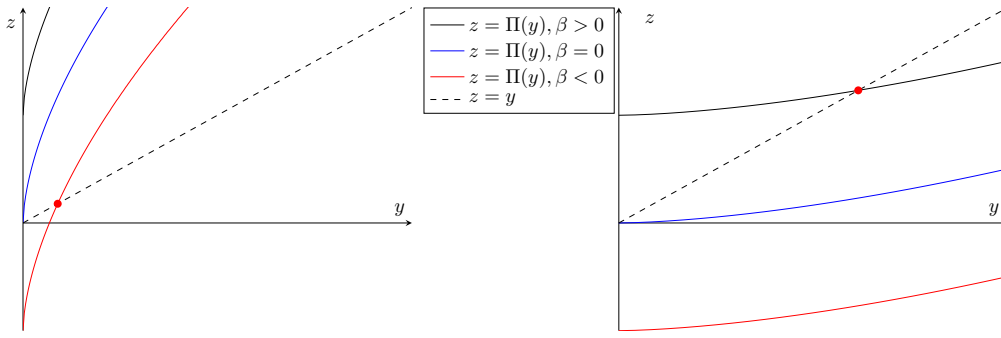
Figure 2.8: Plots of $\Pi(y)$ vs. y from (2.18). We see that fixed points exist in accordance with Theorem 2.3.2. On the left, $\sigma_0 = 1.6$ and on the right, $\sigma_0 = 0.6$.

The Theorem essentially describes the existence and stability of a periodic orbit as a hyperbolic equilibrium of a planar vector field undergoes a homoclinic bifurcation. We lay down a brief sketch of the proof.

Proof. It can be shown that there exists a C^1 equivalence of the flow defined by system (2.16) to that its linearisation around the equilibrium $x_0 = 0$, see [12]. Thus we consider the linear system

$$\begin{cases} \dot{x} = \lambda_1 x, \\ \dot{y} = \lambda_2 y. \end{cases} \tag{2.17}$$

By scaling x and y, we can assume that the homoclinic orbit Γ_0 passes through $(1, 0)$ and then returns back through $(0, 1)$. We define a cross section $\Sigma^s = \{x = 1\}$ across the stable manifold and observe how the orbit returns back to this cross section. We define another cross section $\Sigma^u = \{y = 1\}$. As we are interested in the existence of a periodic orbit, we try to obtain a mapping from Σ_s to itself, see Figure 2.7. A fixed point of the obtained map Π would then correspond to a periodic orbit in system (2.17). We do this by defining two maps:

$$\Pi_{loc} : \Sigma_s \mapsto \Sigma_u,$$

and

$$\Pi_{glob} : \Sigma_u \mapsto \Sigma_s.$$

Then,

$$\Pi = \Pi_{loc} \circ \Pi_{glob}.$$

For Π_{loc} we use the flow (2.17) to obtain a mapping from Σ_s to Σ_u. Thus

$$\Pi_{loc} : y \mapsto y^\nu,$$

where $\nu = -\lambda_1/\lambda_2$ is defined as the *saddle index*. For $\sigma_0 < 0$, $\nu > 1$ and for $\sigma_0 > 0$, $\nu < 1$. The global return map Π_{glob} is a general map mapping $(1, 0)$ to $(0, 1)$ for $\beta = 0$.

$$\Pi_{glob} : x \mapsto \beta + C_1 x + O(x^2).$$

The affine linear term β is the splitting function. The parameter $C_1 > 0$ as orbits cannot intersect each other. Clearly, for $\beta = 0$, Π_{glob} maps $(1, 0)$ to $(0, 1)$, both part of the homoclinic orbit Γ_0. A composition of the two maps gives us the *Poincaré map*,

$$\Pi : y \mapsto \beta + C_1 y^\nu + O(y^{2\nu}).$$

As we analyse the behavior close to the equilibrium $x_0 = 0$, we neglect the higher order terms. The final model map we consider is thus

$$\boxed{\Pi : y \mapsto \beta + C_1 y^\nu.} \tag{2.18}$$

In Figure 2.8 we observe when fixed points exist, depending on β and ν. Via cobweb analysis, we can clearly see that for $\sigma_0 < 0$, the periodic orbit, when it exists, is stable and for $\sigma_0 > 0$, the periodic orbit, when it exists is unstable. $\qquad\square$
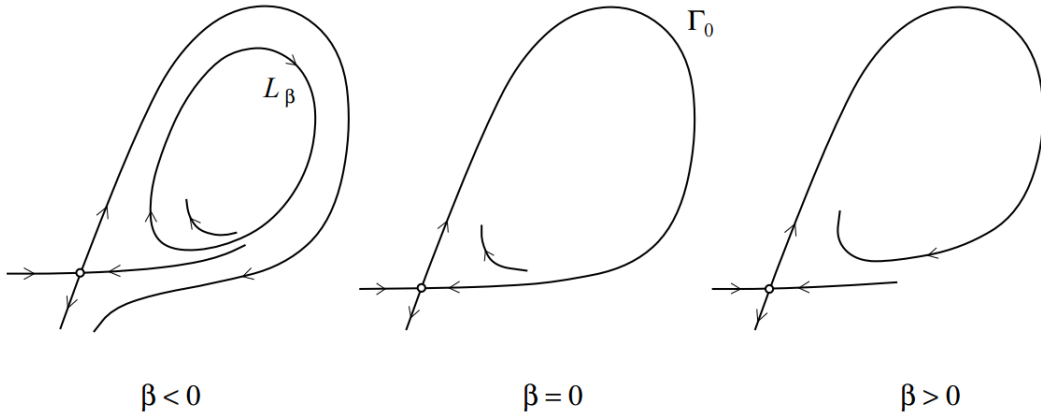
Figure 2.9: Consequence of the Andronov-Leontovich Theorem (2.3.2) for saddle quantity $\sigma_0 > 0$. As the homoclinic connection breaks, we see that an unstable periodic orbit exists for $\beta < 0$, whereas no periodic orbit exists for $\beta > 0$. This is in line with figure Figure 2.8 where via cobweb analysis we can determine that for $\beta > 0$ and $\sigma_0 < 0$ we have a stable periodic orbit and, for $\beta < 0$ and $\sigma_0 < 0$ we have an unstable periodic orbit. Figure taken from [12].

2.3.2 Homoclinic orbit to saddle-focus

We now consider, using the same approach as in the saddle case, homoclinic orbits in 3-dimensional systems. There are thus, two possibilities, either all eigenvalues are real (saddle case) or there exists a pair of complex eigenvalues (the saddle-focus case). If the unstable leading eigenvalue is complex, then by reversing time, we can get the stable leading one to be complex. Thus in general the analysis for a pair of complex eigenvalues in a 3-dimensional system would correspond to the analysis of a saddle-focus.

We do not consider the case where we have three real eigenvalues. The results are the same for $\sigma_0 < 0$ as in the Andronov-Leontovich Theorem, while in the case of $\sigma_0 > 0$, the existence of a periodic orbit depends on the sign of the bifurcation parameter and the topology of the unstable manifold. We do not discuss it further.

Theorem 2.3.2 explains the homoclinic bifurcation in a planar system, where both eigenvalues are real. As a pair of complex eigenvalues in a planar system would correspond to either stable, unstable or non-hyperbolic equilibria, there would be no hyperbolic homoclinic bifurcations in that case. However in the 3-dimensional case, a pair of complex eigenvalues and a real eigenvalue give rise to a saddle-focus, to which homoclinic orbits may exist and undergo bifurcations.

Theorem 2.3.3. *Consider*

$$\dot{x} = f(x, \alpha), \quad x \in \mathbb{R}^3, \; \alpha \in \mathbb{R}, \tag{2.19}$$

such that f is smooth. Let us assume that this system has a saddle-focus equilibrium at $x_0 = 0$ with eigenvalues $\lambda_1(0) > 0 > Re(\lambda_{2,3}) > 0$ and a homoclinic orbit Γ_0. We define the saddle quantity $\sigma_0 = \lambda_1(0) + Re(\lambda_{2,3}) > 0$. We have two cases:

1. *($\sigma_0 < 0$): Genericity condition: $\beta'(0) \neq 0$, where β is the split function and $\lambda_2(0) \neq \lambda_3(0)$. Then (2.19) has a unique and stable periodic orbit in a neighborhood of $\Gamma_0 \cup x_0$ for sufficiently small $|\beta|$.*

2. *($\sigma_0 > 0$): Genericity condition: $\lambda_2(0) \neq \lambda_3(0)$. Then (2.19) has an infinite number of saddle limit cycles in a neighborhood of $\Gamma_0 \cup x_0$ for all sufficiently small $|\beta|$.*

In Case 1, the results are similar to that of the saddle case (Theorem 2.3.2). The interesting thing to note is the infinite number of periodic orbits that appear in the $\sigma_0 > 0$ case (also called the *wild* case), a proof of which we give here.
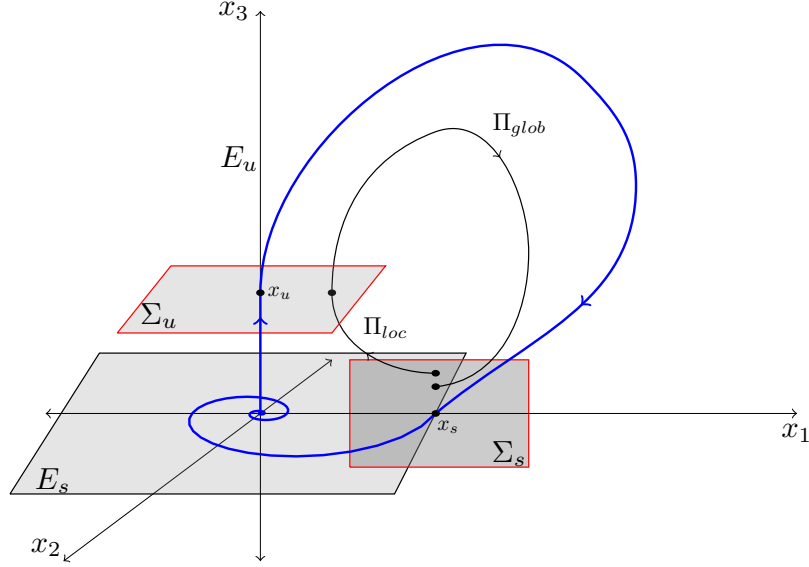
Figure 2.10: Geometric construction for the proof of Theorem 2.3.3.

Proof. (**Case 2**) The proof is in the same spirit as that of Theorem 2.3.2. The geometric construction can be seen in Figure 2.10. We consider a 3-D system

$$\begin{cases} \dot{x_1} = \lambda x_1 + \omega x_2 + f_1(x), \\ \dot{x_2} = -\omega x_1 + \lambda x_2 + f_2(x), \\ \dot{x_3} = \gamma x_3 + f_3(x), \end{cases} \tag{2.20}$$

where $\lambda < 0, \omega > 0$ and $\gamma > 0$, such that the equilibrium $x = 0$ possesses a homoclinic orbit. The Taylor expansions of f_i have zero linear part, for all i. At the critical equilibrium the eigenvalues are $\lambda \pm i\omega$ and γ. Let us also assume that the homoclinic orbit passes through the points $(0, 0, 1)$ and $(1, 0, 0)$. Near the singularity, we consider the linear system,

$$\begin{cases} \dot{x_1} = \lambda x_1 + \omega x_2, \\ \dot{x_2} = -\omega x_1 + \lambda x_2, \\ \dot{x_3} = \gamma x_3, \end{cases}$$

since the flow of (2.20) is C^1 equivalent near the saddle-focus to the flow of the linearisation. Consider Figure 2.10. We construct cross sections Σ_s and Σ_u close to the saddle-focus, transversal to the stable and unstable manifolds respectively. Here

$$\Sigma_s = \{x \ : \ x_2 = 0\},$$

and

$$\Sigma_u = \{x \ : \ x_3 = 1\}.$$

Proceeding in the same way as in the saddle case, we formulate the return map $\Pi : \Sigma_s \mapsto \Sigma_s$ by taking the composition of maps $\Pi_{loc} : \Sigma_s \mapsto \Sigma_u$ and $\Pi_{glob} : \Sigma_u \mapsto \Sigma_s$ which are the local and global return maps respectively.

Let us consider point $x_s = (x_1^s, 0, x_3^s) \in \Sigma_s$ and $x_u = (x_1^u, x_2^u, 1)$. Then the local map Π_{loc} is given by

$$\Pi_{loc} : \begin{pmatrix} x_1^s \\ x_3^s \end{pmatrix} \mapsto \begin{pmatrix} x_1^s (x_3^s)^\nu \cos\left(-\frac{\omega}{\gamma} \ln x_3^s\right) \\ x_1^s (x_3^s)^\nu \sin\left(-\frac{\omega}{\gamma} \ln x_3^s\right) \end{pmatrix},$$
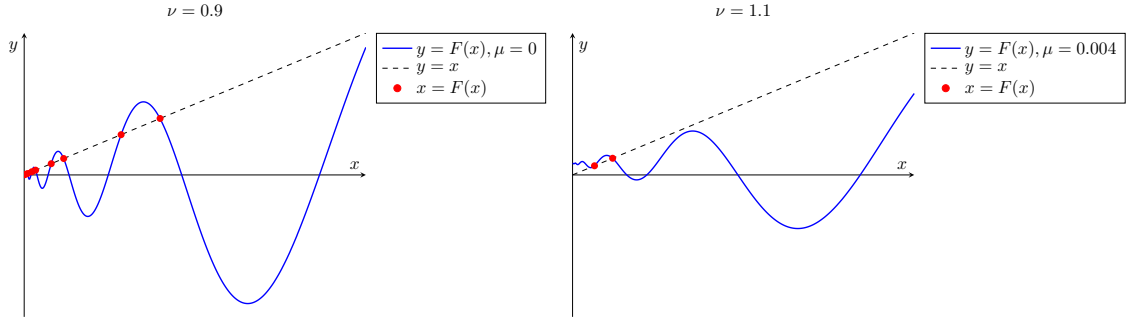
Figure 2.11: Plots of the function (2.21) for $\nu < 1$ and $\nu > 1$. The parameter μ shifts the curve up (down) for positive (negative) values. In the case $\nu < 1$, we see that there exist infinitely many fixed points (and thus periodic orbits) at $\mu = 0$ (the homoclinic orbit) for small values of x. For $|\mu|$ sufficiently small, the infinitely many fixed points persist. In the case $\nu > 1$, for $\mu = 0$ the only fixed point is $x = 0$. For $|\mu|$ and $x > 0$ sufficiently small,it is possible to see finitely many more fixed points, or none at all.

where $\nu = -\lambda/\gamma$ is the saddle index from before.

The global return map Π_{glob} is taken as a general C^1 map from Σ_u to Σ_s such that $(0, 0, 1)$ is mapped to $(1, 0, \beta)$, where β is the splitting function as defined before. Thus, at $\beta = 0$, the returning orbit intersects nontransversally with the stable manifold and becomes homoclinic. Therefore,

$$\Pi_{glob} : \begin{pmatrix} x_1^u \\ x_2^u \end{pmatrix} \mapsto \begin{pmatrix} 1 + ax_1^u + bx_2^u \\ \mu + cx_1^u + dx_2^u \end{pmatrix} + O(\|x^u\|^2),$$

such that $ad - bc \neq 0$ to guarantee local invertibility. Composing the two maps we get

$$\Pi : \begin{pmatrix} x_1^s \\ x_3^s \end{pmatrix} \mapsto \begin{pmatrix} 1 + Ax_1^s(x_3^s)^\nu \sin\left(-\frac{\omega}{\gamma}\ln x_3^s\right) \\ \mu + Bx_1^s(x_3^s)^\nu \sin\left(-\frac{\omega}{\gamma}\ln x_3^s\right) \end{pmatrix} + O(\|x^s\|^2).$$

Thus we have formulated a Poincaré map from Σ_s to itself. The fixed points of this map reveal the bifurcations occuring in a small neighbourhood of $\Gamma_0 \cup x_0$. Therefore the condition for fixed points is:

$$\begin{pmatrix} x_1^s \\ x_3^s \end{pmatrix} = \begin{pmatrix} 1 + Ax_1^s(x_3^s)^\nu \sin\left(-\frac{\omega}{\gamma}\ln x_3^s\right) \\ \mu + Bx_1^s(x_3^s)^\nu \sin\left(-\frac{\omega}{\gamma}\ln x_3^s\right) \end{pmatrix} + O(\|x^s\|^2).$$

Upon replacing the value of x_1^s in the equation for x_3^s, we get

$$x = \mu + x^\nu \sin\left(-\frac{\omega}{\gamma}\ln x\right),$$

where the higher order terms are dropped as we want to observe small $\|x\|$ effects. Also, the (sub)superscripts were dropped. This is the scalar fixed point condition for the saddle-focus case. Note that while performing fixed point analysis we fix ν, γ and ω. We choose small $|\mu|$. We define the map $F(x, \mu)$:

$$\boxed{F : x \mapsto \mu + x^\nu \sin\left(-\frac{\omega}{\gamma}\ln x\right).} \tag{2.21}$$

We readily observe that for $\nu < 1$ ($\sigma_0 > 0$), infinitely many fixed points exist and for $\nu > 1$ ($\sigma_0 < 0$) there are finitely many (at least one) fixed points, for all values of μ sufficiently small, see Figure 2.11. $\square$

2.3.3   Homoclinic Center Manifold

In the previous sections we saw how the one-dimensional fold normal form can be used to explain the fold bifurcation in higher dimensional systems too, with the help of Theorem 2.1.4 and Theorem 2.1.6. The result is different in the case of homoclinic orbits, which can be structurally unstable only in the case of homoclinic orbits to nonhyperbolic equilibria.

Central eigenvalues are defined by the union of the stable and unstable leading eigenvalues. Let us consider

$$\dot{x} = f(x, \alpha), \quad x = (x_1, x_2, ..., x_n) \in \mathbb{R}^n, \quad \alpha \in \mathbb{R}.$$

such that there exists a homoclinic orbit Γ_0 to the equilibrium $x_0 = 0$ at $\alpha = 0$.. Let the corresponding solution be $x^0(t)$. We define the following linear subspaces:

$$E^{uu}(t_0) = \left\{ v_0 \ : \ \lim_{t \to -\infty} \frac{v(t)}{\|v(t)\|} \in T^{uu} \right\},$$

$$E^{ss}(t_0) = \left\{ v_0 \ : \ \lim_{t \to +\infty} \frac{v(t)}{\|v(t)\|} \in T^{ss} \right\},$$

$$E^{cu}(t_0) = \left\{ v_0 \ : \ \lim_{t \to -\infty} \frac{v(t)}{\|v(t)\|} \in T^c \oplus T^{uu} \right\},$$

$$E^{cs}(t_0) = \left\{ v_0 \ : \ \lim_{t \to +\infty} \frac{v(t)}{\|v(t)\|} \in T^c \oplus T^{ss} \right\},$$

Here, $T^{uu}(T^{ss})$ is the nonleading unstable (stable) eigenspace and $T^{cu}(T^{cs})$ is the leading unstable (stable) eigenspace. The function $v(t)$ is a solution of the linearisation around $\Gamma_0 \cup x_0$

$$\begin{cases} \dot{v} = f_x(x^0(t), 0)v + f_\alpha(x^0(t), 0)\mu, \\ \dot{\mu} = 0. \end{cases}$$

with starting data $v = v_0$ and $t = t_0$. Finally, we define

$$E^c(t_0) = E^{cu}(t_0) \cap E^{cs}(t_0).$$

Then, under the conditions,

$\dot{x^0}(0) \in E^c(0)$, and

$E^{uu}(0) \oplus E^c(0) \oplus E^{ss}(0) = \mathbb{R}^n,$

there exists a parameter dependent center manifold M_α defined in a small neighbourhood of $\Gamma_0 \cup x_0$ for sufficiently small $|\alpha|$, such that the manifold is attracting within the neighbourhood and the tangent space for all t_0 is $E^c(t_0)$. The manifold M_α is called the homoclinic center manifold. In general, it is only C^1 smooth.

Once again, we are able to determine the essential changes in the phase portrait as the homoclinic orbit splits for small perturbations of the field, by reducing the problem to looking for the dynamics on the homoclinic center manifold, which is of lower dimension.

Thus, the saddle (saddle-focus) cases presented before can be extended too higher dimensional systems with saddle (saddle-focus) leading eigenvalue configurations. By studying two, three or four dimensional systems with different eigenvalue configurations, we can in principle describe the dynamics of the homoclinic bifurcation in higher dimensional systems too.

Chapter 3

The near-to-saddle model map

In Chapter 1 we introduced the 3DL transition, which is characterised by a specific transition in the leading eigenvalue configurations along a curve of primary homoclinic orbits. These configurations are presented in Figure 3.1.
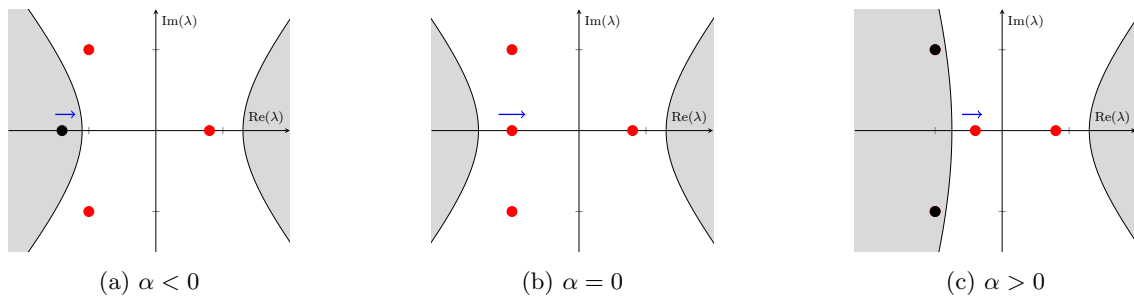
Figure 3.1: 3DL transition: leading eigenvalue configurations

In this chapter we derive a model map that describes bifurcations occurring close to the transition. We consider a generic 4D system with a homoclinic orbit and a 3DL transition, and perform a two-parameter perturbation study on it.

Using Poincaré map techniques, similar to the saddle and saddle-focus cases we are able to derive a model return map describing bifurcations of periodic orbits and secondary homoclinic orbits close to the transition. The map obtained is different from the saddle, saddle-focus or Belyakov cases.

3.1 Construction

We start with a result by Belitskii [3] that will be useful in the derivation.

Theorem 3.1.1. *(Belitskii) There exists a C^1 equivalence of the flow corresponding to a system in $\mathbb{R}^n$ to the flow generated by its linear part near a hyperbolic equilibrium with eigenvalues $\lambda_1, \lambda_2..., \lambda_n$ such that*

$$Re\ \lambda_i \neq\ Re\ \lambda_j +\ Re\ \lambda_k,$$

for all combinations of $i, j, k = 1, 2, ..., n$.

In this derivation we make the following assumptions about the 3DL transition,

    (A.1) The eigenvalues of the linearisation at the critical 3DL saddle are

$$\gamma_0, \gamma_0 \pm i\omega_0 \text{ and } \beta_0,$$

    where $\gamma_0 < 0, \omega_0 > 0$ and $\beta_0 > 0$.

(A.2) There exists a primary homoclinic connection Γ_0 to this 3DL-saddle.

(A.3) The homoclinic orbit Γ_0 satisfies the following genericity condition: The tangent vector v_0 to the portion of Γ_0 which is ϵ-close to the 3DL saddle is either completely spanned by the unstable eigenvector, or spanned by the eigenvectors corresponding to the stable real and complex eigenvalues, with non-zero components.

Without loss of generality, we assume that β_0 is small positive number. This helps us later in the asymptotic analysis of the map we construct.

Now, we describe the model flow, and the Poincaré map close to the 3DL transition, that we will use for a two-parameter perturbation study.

The model flow

For any system satisfying the assumptions **(A.1-3)**, we can transform this system near the critical saddle via a linear transformation to

$$
\begin{cases}
\dot{x_1} = & \gamma(\mu)x_1 - x_2 + f_1(x,\mu,\omega), \\
\dot{x_2} = & x_1 + \gamma(\mu)x_2 + f_2(x,\mu,\omega), \\
\dot{x_3} = & (\gamma(\mu) - \mu_1)\,x_3 + f_3(x,\mu,\omega), \\
\dot{x_4} = & \beta(\mu)x_4 + f_4(x,\mu,\omega).
\end{cases}
\tag{3.1}
$$

The components of $\mu = (\mu_1, \mu_2)$ are small parameters, where μ_2 is a 'splitting parameter' and μ_1 is a small parameter that controls which stable eigenvalue leads. For $\mu_1 > 0$, the stable leading eigenvalue is complex (saddle-focus case) and for $\mu_1 < 0$ the stable leading eigenvalue is real (saddle case). Functions f_1, f_2 and f_3 are nonlinear such that $f_i(0, \mu, \omega) = 0$ for $i = 1, 2, 3, 4$ and $\forall \mu, \omega$. The functions γ, ω and β all depend on μ.

The 3DL saddle exists at $\mu = 0$ and the primary homoclinic connection to all saddles (saddle, 3DL, saddle-focus) exists along the curve $\mu_2 = 0$. The role of μ_2 will become clear later. Thus,

$$
\gamma(0) = \gamma_0, \ \omega(0) = \omega_0 \text{ and } \beta(0) = \beta_0.
\tag{3.2}
$$

For μ_1 sufficiently small, we can use Belitskii's Theorem to get a C^1 equivalence of the flow (3.1) to its linear part, around the equilibrium $O = (0, 0, 0, 0)$. Therefore we consider the following linear system for the rest of the chapter,

$$
\begin{cases}
\dot{x_1} = & \gamma(\mu)x_1 - x_2, \\
\dot{x_2} = & x_1 + \gamma(\mu)x_2, \\
\dot{x_3} = & (\gamma(\mu) - \mu_1)\,x_3, \\
\dot{x_4} = & \beta(\mu)x_4.
\end{cases}
\tag{3.3}
$$

Motivating the use of flow (3.3)

The return of the homoclinic orbit to the saddle is illustrated in Figure 3.3, for three values of the control parameter μ_1. Here the stable part of (3.3) is plotted. The flow corresponding to the stable part of (3.3) is composed of its first three equations. For,

- $\mu_1 < 0$: leading stable eigenspace is real and 1-dimensional (saddle case),

- $\mu_1 = 0$: leading stable eigenspace is 3-dimensional (3DL case), and

- $\mu_1 > 0$: leading stable eigenspace is complex and 2-dimensional (saddle-focus case).

As the orbits approach the origin we observe rotational effects (in the plane spanned by x_1 and x_2) and exponential effects (along x_3). These shapes are based on the nature of leading eigenvalues, which are $\gamma - \mu_1$ and $\gamma \pm i$.

For example, when $\mu_1 = -0.05 < 0$, the leading eigenvalue is real. We see that the oscillations produced by the variables x_1 and x_2 (corresponding to complex eigenvalues) decay faster than the
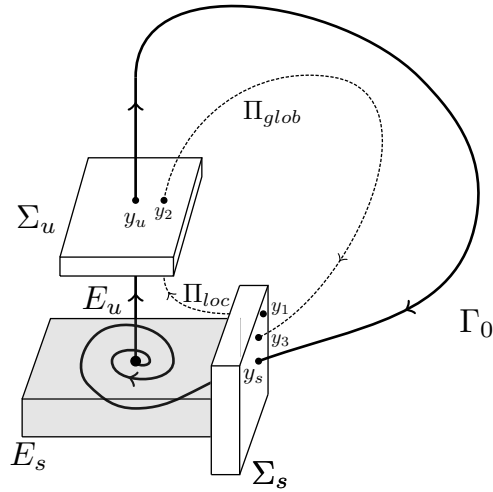
Figure 3.2: The geometric construction of cross sections close to the critical 3DL-saddle at $(0,0,0,0)$ and the homoclinic connection Γ_0, in order to obtain the map $\Pi : \Sigma_s \mapsto \Sigma_s$. Here Σ_u is defined by the cross section $x_4 = 1$ and Σ_s is the cross section $x_3 = 0$. The homoclinic connection is assumed to pass through the points $y_s = (1, 0, 1, 0)$ and $y_u = (0, 0, 0, 1)$. The stable and unstable eigenspaces are E_s and E_u respectively.
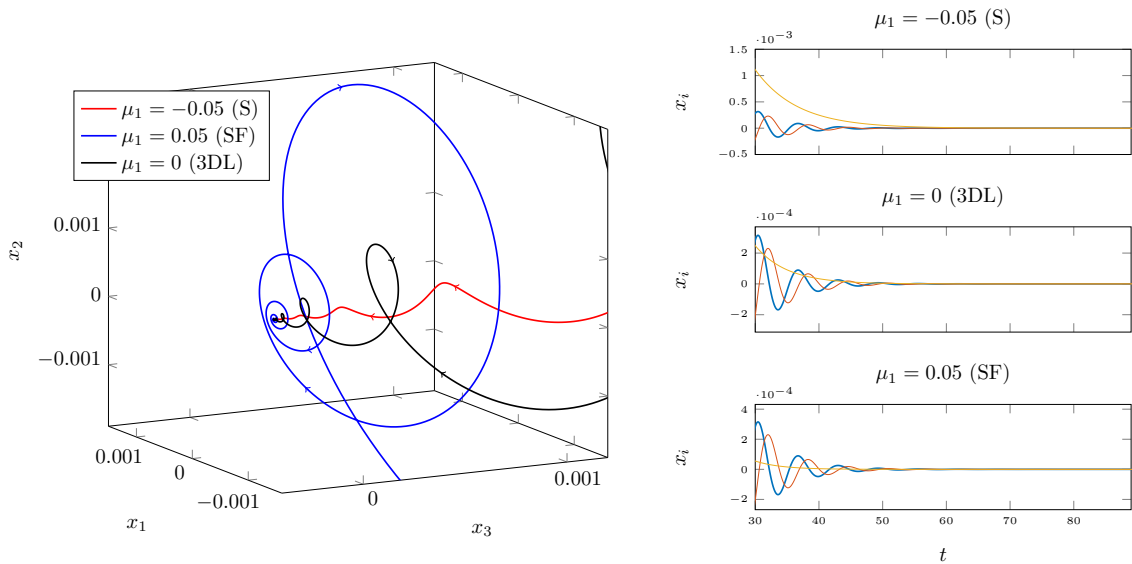
Figure 3.3: Orbits in the stable manifold of the linear system (3.3) for different values of μ_1. Note that the system is decoupled. The parameter μ_1 controls the transition from saddle (S) to 3DL-saddle and, to saddle-focus (SF). All orbits begin from the same point in the stable manifold, close to the origin. In the time series plots, x_1 (blue) x_2 (red) and x_3 (yellow) are plotted against time for the three cases of μ_1.

exponentially decreasing x_3 (corresponding to a real eigenvalue). Thus the homoclinic orbit in this case returns locally along a 1-dimensional manifold, which locally corresponds to the Andronov-Leontovich theorem (Theorem 2.3.2). In the case $\mu_1 > 0$, the reverse happens, x_3 decays faster than the oscillatory x_1 and x_2. Thus the homoclinic orbit in this case approaches the origin locally along a two dimensional manifold. This is the saddle-focus case and locally corresponds to Theorem 2.3.3.

However, in the case $\mu_1 = 0$, the leading eigenspace is three dimensional, and all variables x_1, x_2 and x_3 decay at the same rate. Locally, the homoclinic orbit approaches the origin (3DL saddle) along a three-dimensional manifold.

To summarise, our goal in this chapter is to use flow (3.3) to explain the phase portraits close to the 3DL saddle and the homoclinic orbit, for small perturbations. We do so by introducing cross sections close to the saddle, and deriving a map on these cross sections.

Introducing cross sections

Figure 3.2 gives an impression of the homoclinic connection to a 3DL-saddle in the four-dimensional flow. As we are interested in understanding the bifurcations close to the saddle and the homoclinic orbit, we define two Poincaré cross sections close to this saddle,

$$\Sigma_s = \{(x_1, x_2, x_3, x_4) | x_2 = 0\},$$
$$\Sigma_u = \{(x_1, x_2, x_3, x_4) | x_4 = 1\},$$

and assume that the homoclinic orbit passes through both of these cross sections at $y_s = (1, 0, 1, 0)$ and $y_u = (0, 0, 0, 1)$ respectively.

Clearly, both cross sections are transversal to the flow and to the stable and unstable eigenspaces. Thus, by computing orbits beginning from Σ_s to Σ_u and back to Σ_s we are able to define a three-dimensional map Π mapping Σ_s to itself. This map can then be used to study periodic orbits and secondary homoclinic orbits closeby.

We shall construct the map Π in two parts, $\Pi_{loc} : \Sigma_s \mapsto \Sigma_u$ and $\Pi_{glob} : \Sigma_u \mapsto \Sigma_s$ giving us

$$\Pi = \Pi_{glob} \circ \Pi_{loc}.$$

So far, we have geometrically described a map on a cross section close to the 3DL-saddle. There are two parameters, μ_1 and μ_2 which control the assumptions **(A.1-2)**. Moving μ_1 makes the saddle change from saddle to 3DL-saddle to saddle focus and vice-versa, while μ_2 controls the orientation of the stable manifold. We have a homoclinic connection only for $\mu_2 = 0$. Thus, with the help of these two parameters we can understand the dynamical behaviour at the 3DL-saddle, by observing what happens for small perturbations of the saddle and the homoclinic connection.

3.2   Derivation of the map

We begin by computing the orbit of the flow (3.3) starting from an arbitrary point in Σ_s, close to y_s. This will help us to define the map Π_{loc}. The local map Π_{loc} is thus the mapping from $(x_1^s, 0, x_3^s, x_4^s) \in \Sigma_s$ to a point $(x_1^u, x_2^u, x_3^u, 1)$ on Σ_u close to y_u. The orbit at time t starting from $(x_1^s, 0, x_3^s, x_4^s)$ is thus

$$\begin{pmatrix} x_1(t) \\ x_2(t) \\ x_3(t) \\ x_4(t) \end{pmatrix} = \begin{pmatrix} x_1^s e^{\gamma t} \cos t \\ x_1^s e^{\gamma t} \sin t \\ x_3^s e^{(\gamma - \mu_1) t} \\ x_4^s e^{\beta t} \end{pmatrix}.$$

We then compute the time $t = T_{loc}$ to reach Σ_u (where $x_4 = 1$), which is

$$T_{loc} = -\frac{1}{\beta} \log x_4^s.$$

The map Π_{loc} is given by

$$\Pi_{loc} : \begin{pmatrix} x_1^s \\ x_3^s \\ x_4^s \end{pmatrix} \mapsto \begin{pmatrix} x_1^s (x_4^s)^\nu \cos\left(\frac{-1}{\beta}\log x_4^s\right) \\ x_1^s (x_4^s)^\nu \sin\left(\frac{-1}{\beta}\log x_4^s\right) \\ x_3^s (x_4^s)^{\nu + \mu_1/\beta} \end{pmatrix}. \tag{3.4}$$

where $\nu = -\gamma/\beta$ is defined as the *saddle index*.

For the global return map $\Pi_{glob} : \Sigma_u \mapsto \Sigma_s$, we cannot use the flow (3.3) to define the dynamics on Σ_u after making a global turn away from the critical saddle. Instead we use a general approximation of the flow from $(0, 0, 0, 1)$ to $(1, 0, 1, \mu_2)$. Here μ_2 is the aforementioned splitting parameter. It controls the return of the orbit to the critical saddle. For $\mu_2 = 0$ only, we have a homoclinic connection.

Thus, the following approximation for Π_{glob} is used

$$\Pi_{glob} : \begin{pmatrix} x_1^u \\ x_2^u \\ x_3^u \end{pmatrix} \mapsto \begin{pmatrix} 1 \\ 1 \\ \mu_2 \end{pmatrix} + \begin{pmatrix} a_{11} & a_{12} & a_{13} \\ a_{21} & a_{22} & a_{23} \\ a_{31} & a_{32} & a_{33} \end{pmatrix} \begin{pmatrix} x_1^u \\ x_2^u \\ x_3^u \end{pmatrix} + \begin{pmatrix} O((x_1^u)^2) \\ O((x_2^u)^2) \\ O((x_3^u)^2) \end{pmatrix}, \tag{3.5}$$

where the constants a_i are dependent on μ. For $A = [a_{ij}]$ we also have the condition $\det(A(0)) \neq 0$ which guarantees invertibility of Π_{glob} for μ small enough.

Now, (3.4) and (3.5) in combination give us the full return map Π. As $\Pi = \Pi_{glob} \circ \Pi_{loc}$,

$$\Pi : \begin{pmatrix} x_1^s \\ x_3^s \\ x_4^s \end{pmatrix} \mapsto \begin{pmatrix} 1 + b_1 x_1^s (x_4^s)^\nu \cos\left(\frac{-1}{\beta}\log x_4^s + \theta_1\right) + b_2 x_3^s (x_4^s)^{\nu+\mu_1/\beta} \\ 1 + b_3 x_1^s (x_4^s)^\nu \sin\left(\frac{-1}{\beta}\log x_4^s + \theta_2\right) + b_4 x_3^s (x_4^s)^{\nu+\mu_1/\beta} \\ \mu_2 + b_5 x_1^s (x_4^s)^\nu \sin\left(\frac{-1}{\beta}\log x_4^s + \theta_3\right) + b_6 x_3^s (x_4^s)^{\nu+\mu_1/\beta} \end{pmatrix}, \tag{3.6}$$

where the small $O(\|x\|^{2\nu})$ terms have been truncated. Also,

$$\sin\theta_1 = \frac{-a_{12}}{\sqrt{a_{11}^2 + a_{12}^2}}, \quad \cos\theta_2 = \frac{a_{22}}{\sqrt{a_{21}^2 + a_{22}^2}}, \quad \cos\theta_3 = \frac{a_{32}}{\sqrt{a_{31}^2 + a_{32}^2}},$$
$$b_1 = \sqrt{a_{11}^2 + a_{12}^2}, \quad b_3 = \sqrt{a_{21}^2 + a_{22}^2}, \quad b_5 = \sqrt{a_{31}^2 + a_{32}^2},$$
$$b_2 = a_{13}, \quad b_4 = a_{23}, \quad \text{and} \quad b_6 = a_{33}.$$

Next, we make the smooth invertible transformation $x_4^s \mapsto x_4^s \exp(\theta_3 \beta)$ to eliminate θ_3. We get the map

$$\boxed{\Pi : \begin{pmatrix} x_1 \\ x_3 \\ x_4 \end{pmatrix} \mapsto \begin{pmatrix} 1 + \alpha_1 x_1 x_4^\nu \cos\left(\frac{-1}{\beta}\log x_4 + \phi_1\right) + \alpha_2 x_3 x_4^{\nu+\mu_1/\beta} \\ 1 + \alpha_3 x_1 x_4^\nu \sin\left(\frac{-1}{\beta}\log x_4 + \phi_2\right) + \alpha_4 x_3 x_4^{\nu+\mu_1/\beta} \\ \mu_2 + C_1 x_1 x_4^\nu \sin\left(\frac{-1}{\beta}\log x_4\right) + C_2 x_3 x_4^{\nu+\mu_1/\beta} \end{pmatrix},} \tag{3.7}$$

where

$$\phi_1 = \theta_1 - \theta_3, \qquad\qquad \phi_2 = \theta_2 - \theta_3, \qquad\qquad \alpha_1 = b_1 \exp(\theta_3 \beta \nu),$$

$$\alpha_2 = b_2 \exp((\nu + \mu_1/\beta)\theta_3\beta), \qquad \alpha_3 = b_3 \exp(\theta_3\beta\nu) \qquad \alpha_4 = b_4 \exp((\nu + \mu_1/\beta)\theta_3\beta),$$

$$C_1 = b_5 \exp(\theta_3\beta\nu) \qquad \text{and} \ \ C_2 = b_2 \exp((\nu + \mu_1/\beta)\theta_3\beta).$$

We have dropped the superscript 's' from the coordinate variables for convenience. This is the final form of the map that we will work with ahead.

Now, to analyse periodic orbits close to the homoclinic connection with respect to the critical 3DL-saddle, we look for fixed points of the map (3.7). As explained in Chapter 2, these fixed points would correspond to periodic orbits in the original ODE system. Bifurcations of these fixed points would describe the various local bifurcations of the corresponding periodic orbits.

The fixed point condition for map (3.7) is

$$\begin{pmatrix} x_1 \\ x_3 \\ x_4 \end{pmatrix} = \begin{pmatrix} 1 + \alpha_1 x_1 x_4^\nu \cos\left(\frac{-1}{\beta}\log x_4 + \phi_1\right) + \alpha_2 x_3 x_4^{\nu+\mu_1/\beta} \\ 1 + \alpha_3 x_1 x_4^\nu \sin\left(\frac{-1}{\beta}\log x_4 + \phi_2\right) + \alpha_4 x_3 x_4^{\nu+\mu_1/\beta} \\ \mu_2 + C_1 x_1 x_4^\nu \sin\left(\frac{-1}{\beta}\log x_4\right) + C_2 x_3 x_4^{\nu+\mu_1/\beta} \end{pmatrix}. \tag{3.8}$$

For non-degeneracy, we require that C_1 and C_2 be non-zero real constants. We justify this ahead. Substituting the expressions for x_1 and x_3 from (3.8) in the expression for x_4 we get

$$x_4 = \mu_2 + C_1 (x_4)^\nu \sin\left(\frac{-1}{\beta}\log x_4\right) + C_2 (x_4)^{\nu+\mu_1/\beta} + O(\|x\|^{2\nu}), \tag{3.9}$$

as our one-dimensional fixed point condition. As we observe behavior close to $(1, 0, 1, 0)$ on the cross section Σ_s, we consider only the leading terms of (3.9) and get the following scalar model return map:

$$\boxed{F(x,\mu) : x \mapsto \mu_2 + C_1 x^\nu \sin\left(\frac{-1}{\beta}\log x\right) + C_2 x^{\nu+\mu_1/\beta}.} \tag{3.10}$$

Note that the presence of the extra additive term $C_2 x^{\nu+\mu_1/\beta}$ is what makes this map different from the the scalar model maps describing the saddle, saddle-focus and Belyakov cases.

Genericity conditions

If we were to set C_1 to zero, then we would obtain finitely many fixed points for all values of ν, μ_1, β, μ_2 and C_2. If we set C_2 to zero, we get the saddle-focus model map. Thus for genericity, we keep C_1 and C_2 non-zero.

The following genericity conditions are required for this bifurcation:

(G.1) (from assumption **(A.3)**) The tangent vector v_0 to the portion of Γ_0 which is ϵ-close to the 3DL saddle is either completely spanned by the unstable eigenvector, or spanned by the eigenvectors corresponding to the stable real and complex eigenvalues, with non-zero components.

(G.2) The coefficients C_1 and C_2 of the map (3.10) are non-zero constants.

(G.3) The Jacobian $\det(d\Pi)$ must be non-zero for $\|\mu\|$ sufficiently small, to ensure invertibility.

In the coming chapter we analyse maps (3.10) and (3.7) for bifurcations of their fixed points and present a qualitative bifurcation diagram, supporting the numerical observations with asymptotic results.

Chapter 4

Analysing the scalar model map

In this chapter we use iterations of map (3.10) to obtain a detailed picture of the bifurcations of their fixed points. To stay close to the 3DL saddle, we only analyse the bifurcations for small values of x and μ. We look at two bifurcation sets broadly:

- Primary period doubling (PD) and limit point (LP) bifurcations

- Secondary homoclinic orbits

4.1 PD/LP bifurcations in the scalar model map

Intuitive understanding of the scalar model map

In Figure 4.1 we show plots of the scalar map (3.10) for different values of ν, μ_1 and μ_2. These parameters affect the shape of the curve differently:

- The parameter ν governs the existence of fixed points. We see that for $\nu > 1$, we have at least one fixed point, for all values of β, C_1, C_2, μ_1 and μ_2. For $\nu < 1$, we obtain infinitely many fixed points.

- The function $F(x, \mu)$ is linearly dependent on μ_2 that shifts the whole curve up or down.

- The role of μ_1 is interesting. It governs the shape of the function $y = F(x, \mu)$ with respect to the line $y = x$. For positive μ_1 the structure of the curve does not change much, but we observe significant change in its trend away from the line $y = x$ for $\mu_1 < 0$.

On fixing μ_1, we can immediately conclude the existence of a PD and LP bifurcation if there exist fixed points of $F(x, \mu)$. This is achieved by varying μ_2 such that the derivative of $F(x, \mu)$ with respect to x at the fixed point is -1 or 1. This is possible due to the sinusoidal nature of the curve $y = F(x, \mu)$. For each trough and crest, we obtain a pair of PD and LP points. As we have infinitely such pairs of troughs and crests, we expect to obtain infinitely many PD and LP curves.

The case $\nu < 1$ is interesting, as we obtain infinitely many fixed points (periodic orbits) and expect to get infinitely many bifurcation curves too. For $\nu > 1$, finitely many fixed points exist, which may or may not be for μ_1 sufficiently small. Thus for the remainder of the thesis we consider only the case $\nu < 1$ (called the *wild case*).

Results and observations from continuation

Upon continuing the infinitely many PD and LP points in the $\mu_1 - \mu_2$ parameter space using the continuation package MatcontM [9] we obtain infinitely many PD and LP curves, which form interesting structures. The curves can be seen in Figure 4.2. We make the following observations:

> **(P.1)** The curves exhibit a repeating behaviour: two branches of one PD or LP curve meet to form a *horn*. Infinitely many such horns exist. The sequence of these horns in the $\mu_1 - \mu_2$ space appear to approach $\mu_2 = 0$ asymptotically, which is the curve of primary homoclinic orbits. Also, the tip of the horns always exist entirely in either the second, or third quadrant of the $\mu_1 - \mu_2$ space.
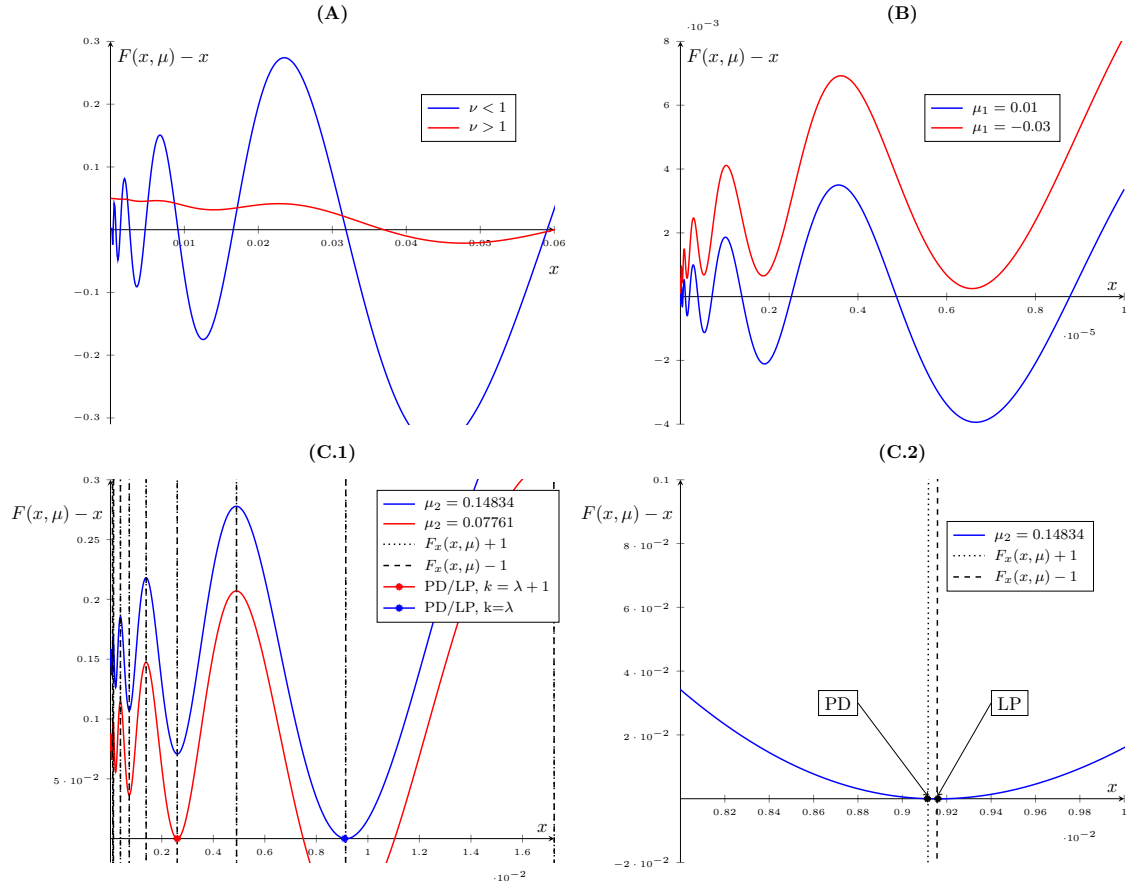
Figure 4.1: Plots of $F(x, \mu) - x$ (from (3.10)) vs. x for different ν, μ_1 and μ_2. We fix $C_1 = 1.7$, $C_2 = -0.3$ and $\beta = 0.2$. In **(A)**, we see that there are infinitely many fixed points (close to zero) when $\nu < 1$. For $\nu > 1$ there exists at least one fixed point away from zero. In **(B)** we see the effect of negative μ_1 on the existence of fixed points when $\nu < 1$. For all positive values of μ_1 we obtain infinitely many fixed points. When $\mu_1 < 0$ we obtain finitely many fixed points for μ_2 sufficiently small. In **(C.1)** we see how infinitely many PD and LP points are obtained. We keep μ_1 fixed and $\nu < 1$. As we decrease μ_2, we locate PD and LP points almost simultaneously for smaller values of x. This can be seen clearly in **(C.2)**, where the derivative of $F(x, \mu)$ changes quickly.

(P.2) The PD and LP curves appear to coincide on visual inspection, and there exist GPD and cusp points in the vicinity of the tip of the horn.

(P.3) The tip of the horn in each of the LP curves is characterised by a cusp point. These cusps always exist, for all values of C_1 and C_2 and form a sequence that appears to approach the origin $\mu = 0$.

(P.4) Upon closer inspection, we observe that there exists either of two subtle structures at the top of every PD/LP horn. One is a *spring area*, where the PD curve forms a loop around the LP cusp before returning. The other is a *saddle area*, where the PD curve makes a sharp turn close to the LP cusp, see Figure 4.3. The spring area is always (generically) accompanied by two GPD points along the PD loop. These points are absent in a saddle area. Mira et al. [15] discuss in detail the spring and saddle areas, including transitions from one case to the other and genericity.

(P.5) The global behaviour of this set of curves depends on parameters C_1 and C_2, which are non-zero.

> **(P.5.1)** For example, by switching the sign of C_2, the set of curves move from the second to the third quadrant of the $\mu_1 - \mu_2$ space, or vice-versa.
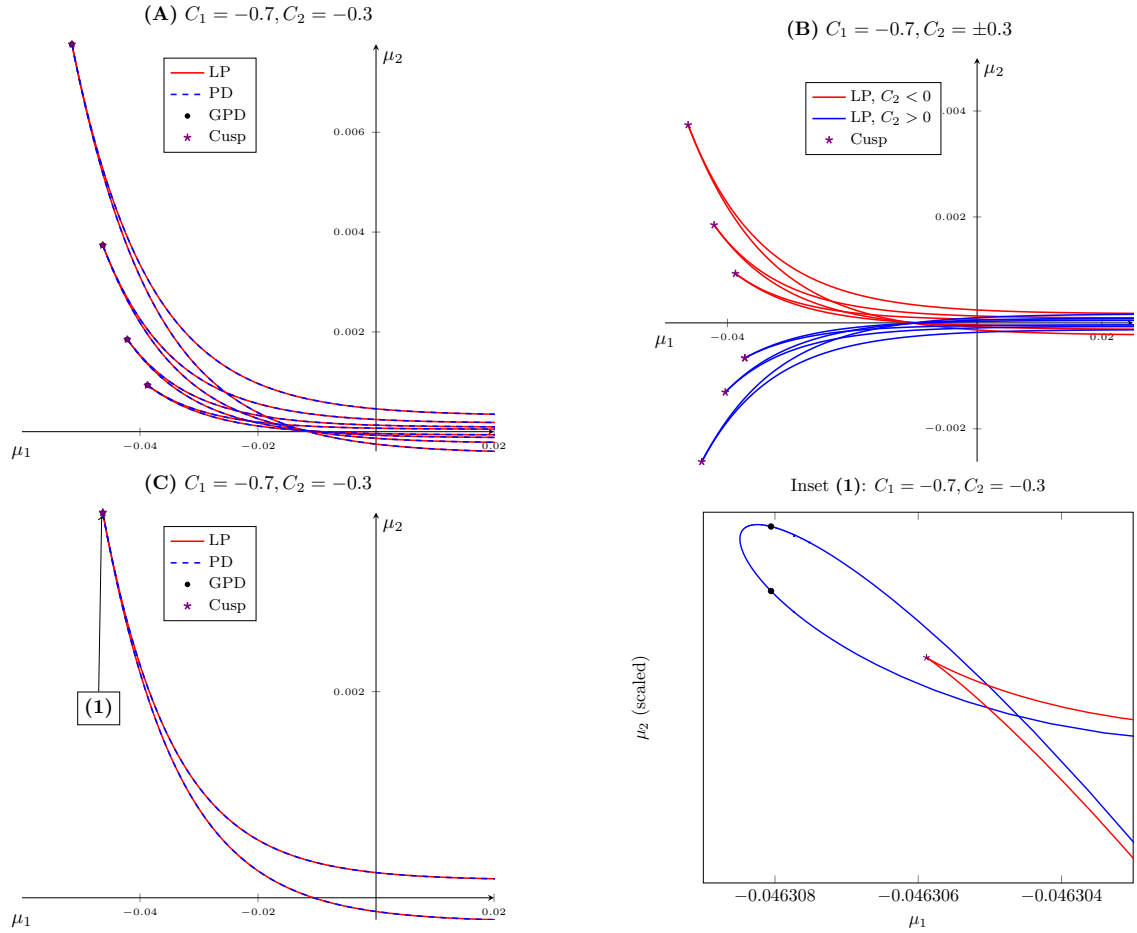
Figure 4.2: Primary PD and LP curves obtained by continuation, for the map (3.10) for a fixed choice of parameters. In **(A)** we plot 4 of these curves. All of them have the same global structure. There are two types of codimension 2 points that can be found along these curves: Cusp (in the case of LP curves) and GPD (in the case of PD curves). In **(B)** we see what happens when we switch the sign of C_2, the *horns* move from $\mu_2 > 0$ to $\mu_2 < 0$. In **(C)** we see one example of a PD/LP curve and spring area (inset).

> **(P.5.2)** The presence of saddle areas or spring areas depend on the parameters C_1 and C_2. The exact domains of separation are not clear.

In the sections ahead we support most of the observations **(P.1-5)** by looking at analytical expressions of the asymptotics of (3.10). The strategy is to look for expressions describing approximate solutions of the PD and LP conditions and use them to justify the observations above for different cases of parameters C_1 and C_2.

4.1.1   Asymptotics: PD/LP curves

In this section we derive approximate solutions to the PD and LP conditions, and use them to justify observations **(P.1-5)**. As we are interested in solutions close to the 3DL bifurcation point $(\mu_1, \mu_2) = (0, 0)$ we assume that x, μ_1 and μ_2 are sufficiently small. As we observe only the wild case we also have the condition

$$\nu < 1.$$
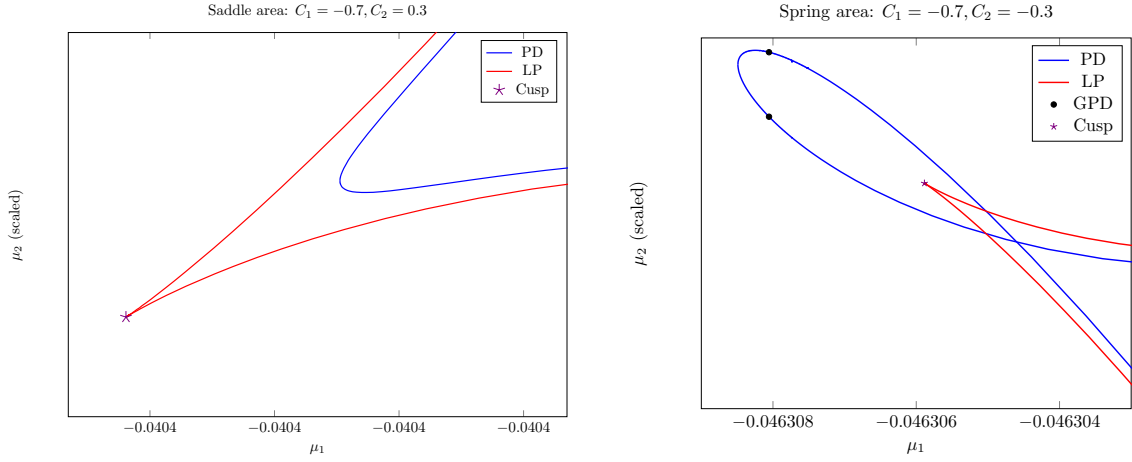
Figure 4.3: Plots of spring and saddle areas for the map (3.10) for different values of C_1 and C_2.

Asymptotic curves

The PD and LP conditions are given by,

$$
\begin{cases}
F(x,\mu) = x, \\
F_x(x,\mu) = -1,
\end{cases}
\text{(PD)} \qquad \text{and} \qquad
\begin{cases}
F(x,\mu) = x, \\
F_x(x,\mu) = 1,
\end{cases}
\text{(LP)} \qquad (4.1)
$$

where $F(x,\mu)$ is given by (3.10). Thus we have,

$$
\begin{cases}
\mu_2 + C_1 x^\nu \sin\left(-\frac{1}{\beta}\log x\right) + C_2 x^{\nu+\mu_1/\beta} = x, \\
x^{\nu-1}\left[\nu C_1 \sin\left(-\frac{1}{\beta}\log x\right) - \frac{C_1}{\beta}\cos\left(-\frac{1}{\beta}\log x\right)\right] + C_2\left(\nu + \mu_1/\beta\right) x^{\nu+\mu_1/\beta-1} = -1,
\end{cases}
\tag{4.2}
$$

for the PD condition and

$$
\begin{cases}
\mu_2 + C_1 x^\nu \sin\left(-\frac{1}{\beta}\log x\right) + C_2 x^{\nu+\mu_1/\beta} = x, \\
x^{\nu-1}\left[\nu C_1 \sin\left(-\frac{1}{\beta}\log x\right) - \frac{C_1}{\beta}\cos\left(-\frac{1}{\beta}\log x\right)\right] + C_2\left(\nu + \mu_1/\beta\right) x^{\nu+\mu_1/\beta-1} = 1,
\end{cases}
\tag{4.3}
$$

for the LP condition.

If we multiply the second equations of (4.2) and (4.3) by $x^{1-\nu} \neq 0$, we get

$$
\nu C_1 \sin\left(-\frac{1}{\beta}\log x\right) - \frac{C_1}{\beta}\cos\left(-\frac{1}{\beta}\log x\right) + C_2\left(\nu + \mu_1/\beta\right) x^{\mu_1/\beta} + x^{1-\nu} = 0, \quad \text{(PD)}
$$

and

$$
\nu C_1 \sin\left(-\frac{1}{\beta}\log x\right) - \frac{C_1}{\beta}\cos\left(-\frac{1}{\beta}\log x\right) + C_2\left(\nu + \mu_1/\beta\right) x^{\mu_1/\beta} - x^{1-\nu} = 0. \quad \text{(LP)}
$$

$$(4.4)$$

Here, the term $x^{1-\nu}$ is very small compared to the rest of the terms as x is small and $\nu < 1$. Thus the leading terms of both, PD and LP conditions are the same. This explains observation **(P.2)** that the PD and LP curves appear to coincide. We can write both conditions of (4.4) together as

$$
\begin{cases}
\mu_2 + C_1 x^\nu \sin\left(-\frac{1}{\beta}\log x\right) + C_2 x^{\nu+\mu_1/\beta} = x, \\
\nu C_1 \sin\left(-\frac{1}{\beta}\log x\right) - \frac{C_1}{\beta}\cos\left(-\frac{1}{\beta}\log x\right) + C_2\left(\nu + \mu_1/\beta\right) x^{\mu_1/\beta} = 0.
\end{cases}
\tag{4.5}
$$

As x is small, $-\frac{1}{\beta}\log x$ will be a large positive number. Thus, we let

$$-\frac{1}{\beta}\log x = \pi n + \theta, \tag{4.6}$$

with $n \in \mathbb{N}$ sufficiently large and $\theta \in (-\pi/2, \pi/2)$. Therefore (4.5) becomes

$$\begin{cases} \mu_2 + C_1 e^{-\nu\beta(\pi n+\theta)}\left[(-1)^n \sin\theta + C_2 e^{-\mu_1(\pi n+\theta)}\right] = e^{-\beta(\pi n+\theta)}, \\ C_1(-1)^n\left[\nu\sin\theta - \frac{1}{\beta}\cos\theta\right] + C_2\left(\nu + \mu_1/\beta\right)e^{-\mu_1(\pi n+\theta)} = 0. \end{cases} \tag{4.7}$$

Consider the second equation of (4.7). We divide both sides by $C_1(-1)^n\nu \neq 0$, giving

$$\sin\theta - \frac{1}{\nu\beta}\cos\theta = (-1)^{n+1}\frac{C_2}{C_1}\frac{\nu + \mu_1/\beta}{\nu}e^{-\mu_1(\pi n+\theta)}. \tag{4.8}$$

Here we make two approximations, assuming μ_1 is chosen to be sufficiently small. Firstly, it follows that the ratio $\frac{\nu+\mu_1/\beta}{\nu} \approx 1$ and secondly, $e^{-\mu_1(\pi n+\theta)} \approx 1$. Thus (4.8) becomes,

$$\sin\theta - \frac{1}{\nu\beta}\cos\theta = (-1)^{n+1}\frac{C_2}{C_1}. \tag{4.9}$$

We can compute $\sin\theta$ from here, which is

$$\sin\theta = \frac{\beta^2\nu^2 C_2^2(-1)^{n+1} \pm \sqrt{C_1^2\left(\beta^2\nu^2 + 1\right) - \beta^2\nu^2 C_2^2}}{C_1\left(\beta^2\nu^2 + 1\right)}. \tag{4.10}$$

Recall that in the previous chapter we assumed β to be a small positive number. This assumption helps in the asymptotics. As $\nu < 1$, the term $\beta\nu$ is a small positive fraction too. Thus the expression for $\sin\theta$ in (4.10) is dominated by the square root term. Thus we get two values of θ,

$$\theta_\pm \approx \pm\arcsin\left(\frac{\sqrt{C_1^2\left(\beta^2\nu^2 + 1\right) - \beta^2\nu^2 C_2^2}}{C_1\left(\beta^2\nu^2 + 1\right)}\right). \tag{4.11}$$

Without loss of generality, we take

$$\boxed{\theta_\pm = \pm\arcsin\left(\frac{\sqrt{C_1^2\left(\beta^2\nu^2 + 1\right) - \beta^2\nu^2 C_2^2}}{|C_1|\left(\beta^2\nu^2 + 1\right)}\right).} \tag{4.12}$$

Now that we have θ, we get two branches for every n,

$$\boxed{\mu_2^{(n,\theta_\pm)} = -e^{-\nu\beta(\pi n+\theta_\pm)}\left[(-1)^n C_1 \sin\theta_\pm + C_2 e^{-\mu_1(\pi n+\theta_\pm)}\right] + e^{-\beta(\pi n+\theta_\pm)}.} \tag{4.13}$$

Choosing the correct n

Next we locate the correct values of n. We observe that for every alternate value of $n \in \mathbb{N}$ the two branches $\mu_2^{(n,\theta_\pm)}$ intersect, and approximate a single PD/LP curve. This can be seen in figure Figure 4.4. Here, the two branches together approximate one horn of the set of PD/LP curves. However, the choice of n ($n = 2k + 1$ or $n = 2k$, $k \in \mathbb{N}$) depends on the parameters C_1 and C_2. The dependency can be seen in the way two branches approximating a single PD/LP curve intersect.

Let us consider branches $\mu_2^{(n,\theta_+)}$ and $\mu_2^{(n,\theta_-)}$ which approximate one PD/LP curve. The condition for their intersection is

$$\mu_2^{(n,\theta_+)} = \mu_2^{(n,\theta_-)}, \tag{4.14}$$

where $\theta_\pm$ are obtained from (4.12). From (4.6) we know that the corresponding values of x are given by

$$x_+ = e^{(-\beta(\pi n+\theta_+))}, \text{ and } x_- = e^{(-\beta(\pi n+\theta_-))} = e^{(-\beta(\pi n-\theta_+))}. \tag{4.15}$$

Using the expressions x_+ and x_-, we combine (4.13) and (4.14) to get

$$- x_+^\nu \left[(-1)^n C_1 \sin \theta_+ + C_2 x_+^{\mu_1/\beta} \right] = -x_-^\nu \left[(-1)^{n+1} C_1 \sin \theta_+ + C_2 x_-^{\mu_1/\beta} \right],$$

$$\implies (-1)^{n+1} C_1 \sin \theta \left(x_+^\nu + x_-^\nu \right) + (x_+ - x_-) = C_2 \left[x_+^{\nu+\mu_1/\beta} - x_-^{\nu+\mu_1/\beta} \right]. \qquad (4.16)$$

Now, we know that

$$x_- = e^{-\beta(\pi n - \theta_+)}$$
$$= e^{-\beta(\pi n + \theta_+ - 2\theta_+)}$$
$$= x_+ e^{2\beta\theta_+}.$$

Replacing the above equation for x_- in (4.16) we get,

$$(-1)^{n+1} C_1 \sin \theta x_+^\nu (1 + e^{2\nu\beta\theta_+}) + x_+ (1 - e^{2\beta\theta_+}) = C_2 x_+^\nu x_+^{\mu_1/\beta} \left(1 - e^{2\nu\beta\theta_+} e^{2\mu_1\theta_+} \right),$$

and we find

$$(-1)^{n+1} \frac{C_1}{C_2} \sin \theta \left(\frac{1 + e^{2\nu\beta\theta_+}}{1 - e^{2\nu\beta\theta_+}} \right) + \frac{x_+^{1-\nu}}{C_2} \left(\frac{1 - e^{2\beta\theta_+}}{1 - e^{2\nu\beta\theta_+}} \right) = x_+^{\mu_1/\beta}, \qquad (4.17)$$

where $e^{2\mu_1\theta_+}$ is assumed to be 1 for μ_1 sufficiently small. Now the term on the left is dominated by $(-1)^{n+1} \frac{C_1}{C_2} \sin \theta \left(\frac{1 + e^{2\nu\beta\theta_+}}{1 - e^{2\nu\beta\theta_+}} \right)$ as $x_+^{1-\nu}$ is small. Also, the RHS is positive, implying that

$$(-1)^{n+1} \frac{C_1}{C_2} \underbrace{\sin \theta}_{>0} \overbrace{\left(\frac{1 + e^{2\nu\beta\theta_+}}{1 - e^{2\nu\beta\theta_+}} \right)}^{<0} > 0.$$

Thus n must be chosen in a way that $(-1)^{n+1} \frac{C_1}{C_2} < 0$. We get

$$\boxed{n = 2k + \frac{1}{2} \left(1 - \mathrm{sgn} \left(\frac{C_1}{C_2} \right) \right),} \qquad (4.18)$$

where $k \in \mathbb{N}$. Equations (4.12),(4.13) and (4.18) give the asymptotic approximation to the set of PD/LP curves obtained from fixed points of the map (3.10).

Explaining observations (P.1-5)

Now that we have the asymptotics, we can explain some of the observations **(P.1-5)**. Clearly, as $k \in \mathbb{N}$, we obtain an infinite sequence of horns. Consider (4.13). In the limit $n \to \infty$, $\mu_2^{(n,\theta_\pm)} \to 0$, as,

$$\lim_{n \to \infty} x = \lim_{n \to \infty} e^{-\beta(\pi n + \theta_\pm)} = 0.$$

This implies that the set of PD/LP curves approach the curve of primary homoclinic orbits $\mu_2 = 0$. Thus we are able to explain observation **(P.1)**.

In Figure 4.2 we also observed that upon switching the sign of C_2, the horns move from the second quadrant to the third quadrant or vice-versa. Indeed, if we combine (4.13) and (4.17), we get

$$\mu_2^{(n,\theta_+)} \approx -x_+^\nu \left[C_1 (-1)^n \sin \theta + (-1)^{n+1} C_1 \sin \theta \left(\frac{1 + e^{2\nu\beta\theta_+}}{1 - e^{2\nu\beta\theta_+}} \right) \right] + x_+,$$

as the expression for the value of μ_2 where two PD/LP branches intersect. Here we drop the small $x^{1-\nu}$ term. By simplifying the expression, we get

$$\mu_2^{(n,\theta_+)} = x_+^\nu (-1)^{n+1} C_1 \sin \theta \left[1 + \left(\frac{1 + e^{2\nu\beta\theta_+}}{-1 + e^{2\nu\beta\theta_+}} \right) \right] + x_+,$$

(A): $C_1 = -0.7$, $C_2 = -0.3$, $k = 10, 14, ..., 60$
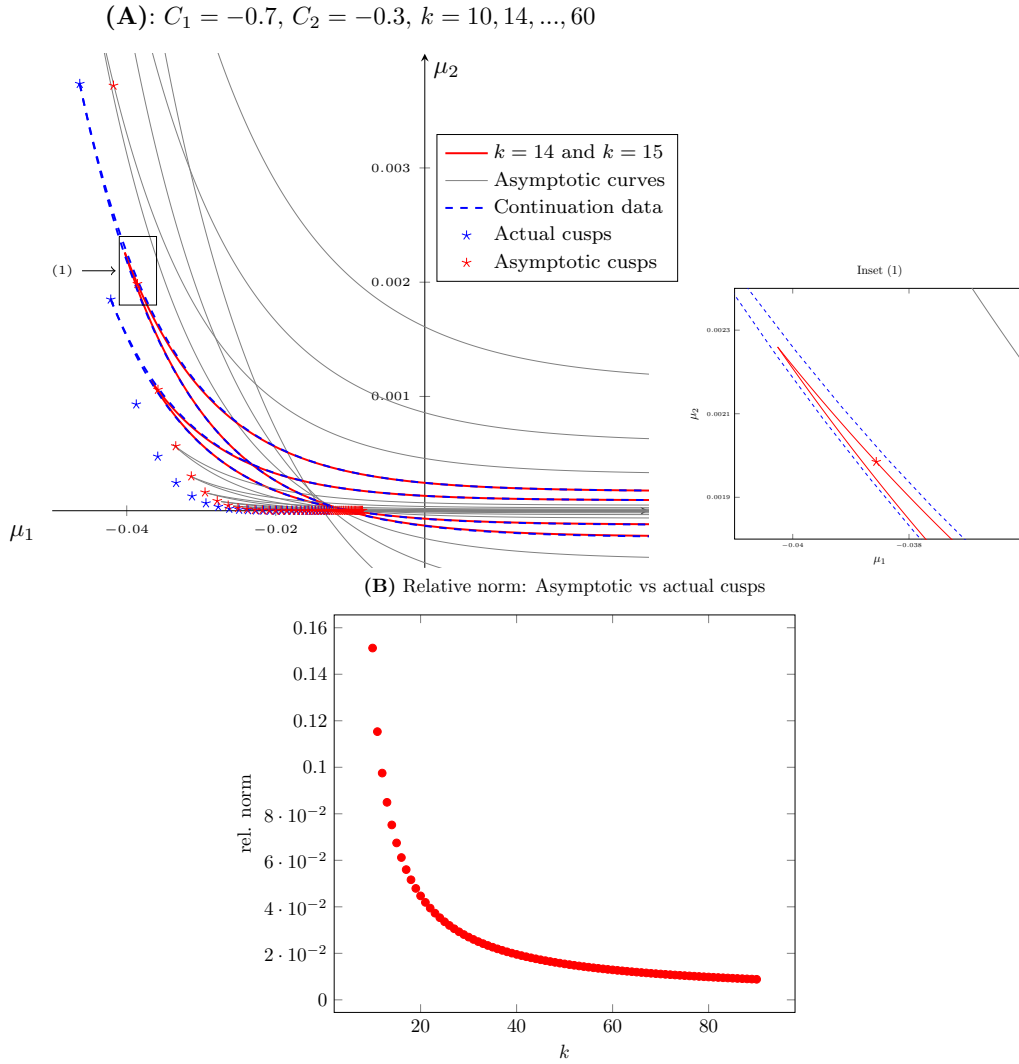
Figure 4.4: Plots of asymptotic curves and PD/LP curves (obtained from continuation). In **(A)** we see how successive asymptotic curves in k approximate the set of PD/LP curves. Here, cusps are obtained by performing Newton iterations to the defining system of the cusp bifurcation with starting points as the asymptotic cusps. In **(B)**, convergence of the asymptotic cusps to the actual cusps is observed. The corresponding values of k in both plots are $k = 10, 11..., 90$.

$$\approx \underbrace{x_+^\nu}_{>0} (-1)^{n+1} C_1 \underbrace{\sin\theta}_{>0} \underbrace{\left[1 + \left(\frac{1+e^{2\nu\beta\theta_+}}{-1+e^{2\nu\beta\theta_+}}\right)\right]}_{>0},$$

as the first x^ν term dominates x. Thus, the sign of $\mu_2^{(n,\theta_+)}$ depends on the sign of $(-1)^{n+1}C_1$. From (4.18), we know that

$$(-1)^{n+1}\frac{C_1}{C_2} = -\left|\frac{C_1}{C_2}\right|,$$

$$\implies (-1)^{n+1}C_1 = -C_2\left|\frac{C_1}{C_2}\right|.$$

Thus, if we switch the sign of C_2, the horns move from $\mu_2 > 0$ to $\mu_2 < 0$ or vice-versa. This explains observation **(P.5.1)**.

4.1.2   Asymptotic sequence of cusp points

In this section we formulate an asymptotic sequence of cusp points by looking at solutions of the defining system for the cusp bifurcation

$$\begin{cases} F(x,\mu) = 0, \\ F_x(x,\mu) - 1 = 0, \\ F_{xx}(x,\mu) = 0, \end{cases} \tag{4.19}$$

where $F(x,\mu) = 0$ is from (3.10). Consider $F_{xx}(x,\mu) = 0$. Dividing both sides by $x^{\nu-2} \neq 0$ we get,

$$C_1\left(\nu(\nu-1) - \frac{1}{\beta^2}\right)\sin\left(-\frac{1}{\beta}\log x\right) - \frac{C_1}{\beta}(2\nu-1)\cos\left(-\frac{1}{\beta}\log x\right)$$
$$+ C_2 x^{\mu_1/\beta}(\nu + \mu_1/\beta)(\nu + \mu_1/\beta - 1) = 0. \tag{4.20}$$

As before, we use the substitution for x,

$$-\frac{1}{\beta}\log x = \pi n + \theta, \tag{4.21}$$

where $n \in \mathbb{N}$ is sufficiently large and $\theta \in (-\pi/2, \pi/2)$. Replacing and simplifying (4.20), we get

$$\sin\theta - \frac{\beta(2\nu-1)}{\beta^2\nu(\nu-1) - 1}\cos\theta = (-1)^{n+1}\frac{C_2}{C_1}e^{-\mu_1(\pi n + \theta)}\left(\frac{(\beta\nu + \mu_1/)(\beta(\nu-1) + \mu_1)}{\beta^2\nu(\nu-1) - 1}\right). \tag{4.22}$$

From this equation, we would like to obtain a concise expression for θ. For μ_1 sufficiently small, we may assume

$$e^{-\mu_1(\pi n + \theta)} \approx 1, \quad \text{and} \quad \left(\frac{(\beta\nu + \mu_1)(\beta(\nu-1) + \mu_1)}{\beta^2\nu(\nu-1) - 1}\right) \approx \left(\frac{\beta^2\nu(\nu-1)}{\beta^2\nu(\nu-1) - 1}\right).$$

Thus, (4.22) becomes

$$\sin\theta - \frac{\beta(2\nu-1)}{\beta^2\nu(\nu-1) - 1}\cos\theta = (-1)^{n+1}\frac{C_2}{C_1}\left(\frac{\beta^2\nu(\nu-1)}{\beta^2\nu(\nu-1) - 1}\right). \tag{4.23}$$

From this expression we obtain $\sin\theta$:

$$\sin\theta \approx \frac{\pm\sqrt{(\beta - 2\beta\nu)^2\left(C_1^2\left(\beta^2(\nu-1)^2 + 1\right)\left(\beta^2\nu^2 + 1\right) - \beta^4 C_2^2(\nu-1)^2\nu^2\right)}}{C_1\left(\beta^2(\nu-1)^2 + 1\right)\left(\beta^2\nu^2 + 1\right)}, \tag{4.24}$$

where $O(\beta^4\nu^4)$ terms from the numerator were ignored. Clearly, as $\beta\nu$ is a small positive number, $|\sin\theta| < 1$. We pick positive θ from (4.24), as we are interested in one cusp point for every LP curve. Thus,

$$\theta = \arcsin\left(\frac{\sqrt{(\beta - 2\beta\nu)^2\left(C_1^2\left(\beta^2(\nu - 1)^2 + 1\right)(\beta^2\nu^2 + 1) - \beta^4 C_2^2(\nu - 1)^2\nu^2\right)}}{|C_1|\left(\beta^2(\nu - 1)^2 + 1\right)(\beta^2\nu^2 + 1)}\right). \tag{4.25}$$

Now that we have θ, we obtain μ_1 and μ_2 from the first two equations of (4.19). Replacing $x = e^{-\beta(\pi n + \theta)}$ in $F_x(x, \mu) = 1$ from (4.19), we get (4.8) once again:

$$(-1)^{n+1}\frac{C_2}{C_1}\underbrace{\frac{\nu + \mu_1/\beta}{\nu}}_{\approx 1}e^{-\mu_1(\pi n + \theta)} = \sin\theta - \frac{1}{\nu\beta}\cos\theta,$$

$$\implies \mu_1 = -\frac{1}{\pi n + \theta}\log\left[(-1)^{n+1}\frac{C_1}{C_2}\left(\sin\theta - \frac{1}{\nu\beta}\cos\theta\right)\right], \tag{4.26}$$

and from $F(x, \mu) = x$ we get

$$\mu_2 = -e^{-\nu\beta(\pi n + \theta)}\left[(-1)^n C_1\sin\theta + C_2 e^{-\mu_1(\pi n + \theta)}\right] + e^{-\beta(\pi n + \theta)}. \tag{4.27}$$

This gives a sequence of asymptotic cusp points

$$\begin{pmatrix}\mu_1^{(n)}\\\mu_2^{(n)}\end{pmatrix} = \begin{pmatrix}-\frac{1}{\pi n + \theta}\log\left[(-1)^{n+1}\frac{C_1}{C_2}\left(\sin\theta - \frac{1}{\nu\beta}\cos\theta\right)\right]\\-e^{-\nu\beta(\pi n + \theta)}\left[(-1)^n C_1\sin\theta + C_2 e^{-\mu_1(\pi n + \theta)}\right] + e^{-\beta(\pi n + \theta)}\end{pmatrix}. \tag{4.28}$$

Choosing the correct value of n

It remains to be verified if the expression in the log term for $\mu_1^{(n)}$ is positive. From the verification we also obtain the correct choice for the sequence of naturals, n. Thus we need to check if

$$(-1)^{n+1}\frac{C_1}{C_2}\left(\sin\theta - \frac{1}{\nu\beta}\cos\theta\right) > 0.$$

We know that $\sin\theta$ is obtained from (4.23). If we replace $\sin\theta$ above, by the expression for $\sin\theta$ from (4.23), we get, upon simplifying, the condition

$$\frac{\left[(-1)^{n+1}\frac{C_1}{C_2}\cos\theta\right](1 + \beta^2\nu^2) + \beta^3\nu(\nu - 1)}{\nu\beta(\beta^2\nu(\nu - 1) - 1)} > 0. \tag{4.29}$$

As $0 < \nu < 1$, the condition reduces to

$$(-1)^{n+1}\frac{C_1}{C_2}\cos\theta < 0. \tag{4.30}$$

This results in the same choice for n as in the case of asymptotic PD/LP curves,

$$n = 2k + \frac{1}{2}\left(1 - \text{sgn}\left(\frac{C_1}{C_2}\right)\right), \tag{4.31}$$

where $k \in \mathbb{N}$.

Cusps asymptotically approach $\mu = 0$

The results can be seen in Figure 4.4. In plot **(B)**, the actual and asymptotic cusps appear to converge in relative norm. Thus, for large values of k, the asymptotic cusps are numerically demonstrated to be a good approximation of the actual cusps. This confirms that the sequence of cusps converge to the origin (3DL bifurcation), as the limit of the sequence (4.28) as $k \to \infty$ is $\mu = 0$. Thus we have an explanation for observation **(P.3)**.

4.1.3 Spring area to saddle area transition

We know that generically, presence of a spring area is accompanied by two GPD points and these points disappear when there is a saddle area [15]. Thus insight about spring area to saddle area transitions may be obtained by analysing the defining system for the GPD bifurcation:

$$
\begin{cases}
F(x, \mu) = 0, \\
F_x(x, \mu) + 1 = 0, \\
\frac{1}{4} \left(F_{xx}(x, \mu) \right)^2 + \frac{1}{6} F_{xxx}(x, \mu) = 0.
\end{cases}
\tag{4.32}
$$

This would answer observation **(P.5.2)**. However, we do not investigate this in the work presented here.
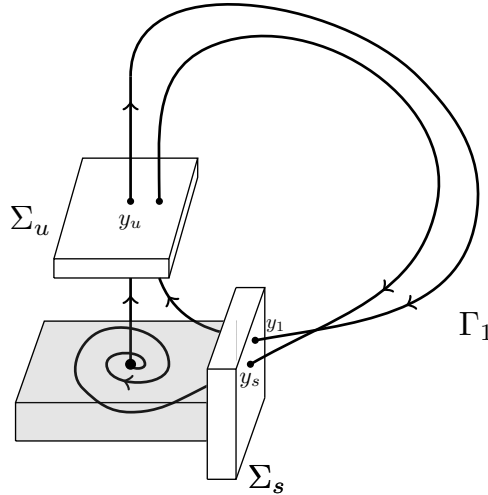
Figure 4.5: Poincaré map for the secondary homoclinic solution Γ_1. Upon leaving y_u along the unstable manifold, the corresponding orbit makes two global turns and returns to the origin.

4.2 Secondary homoclinic orbits

In this section we describe the behaviour of a particular type of homoclinic orbit, namely the *secondary* homoclinic orbit, which, after leaving the saddle along the unstable manifold, makes two global turns and returns to the saddle.

We look at the existence and behaviour of these homoclinic orbits close to the primary homoclinic orbit, upon perturbing the system with parameters μ_1 and μ_2. The existence of the orbits is a codimension 1 situation and would correspond to a curve in the $\mu_1 - \mu_2$ space. As before, we look for these curves in the wild case, where $\nu < 1$.

Consider Figure 4.5. The secondary homoclinic orbit Γ_1 leaves the point $y_u = (0, 0, 0, 1) \in \Sigma_u$, along the unstable manifold and meets Σ_s at $y_1 = (1, 0, 1, \mu_2)$. From this point, the orbit leaves again and this time returns along the stable manifold to approach the origin. The orbit crosses Σ_s at $y_s = (1, 0, 1, 0)$. Using the map Π from (3.7), the condition is,

$$\Pi \begin{pmatrix} 1 \\ 1 \\ \mu_2 \end{pmatrix} = \begin{pmatrix} 1 \\ 1 \\ 0 \end{pmatrix},$$

which gives us the equation

$$\boxed{\mu_2 + C_1 \mu_2^\nu \sin\left(-\frac{1}{\beta} \log \mu_2\right) + C_2 \mu_2^{\nu + \mu_1/\beta} = 0.} \tag{4.33}$$

We define

$$G(\mu) = \mu_2 + C_1 \mu_2^\nu \sin\left(-\frac{1}{\beta} \log \mu_2\right) + C_2 \mu_2^{\nu + \mu_1/\beta}.$$

Note that here μ_2 must be positive. The shape of $G(\mu) = 0$ is similar to the curve $F(x, \mu) = 0$ (from (3.10)). For positive μ_1, it is possible to obtain infinitely many solutions of (4.33) for μ_2 sufficiently small. That is not the case when $\mu_1 < 0$, as there are only finitely many or no non-trivial solutions for μ_2 sufficiently small, see Figure 4.6.

In Figure 4.7 the non-trivial solutions are continued with respect to the parameters μ_1 and μ_2 for two different sets of values of C_1 and C_2. We observe three things:
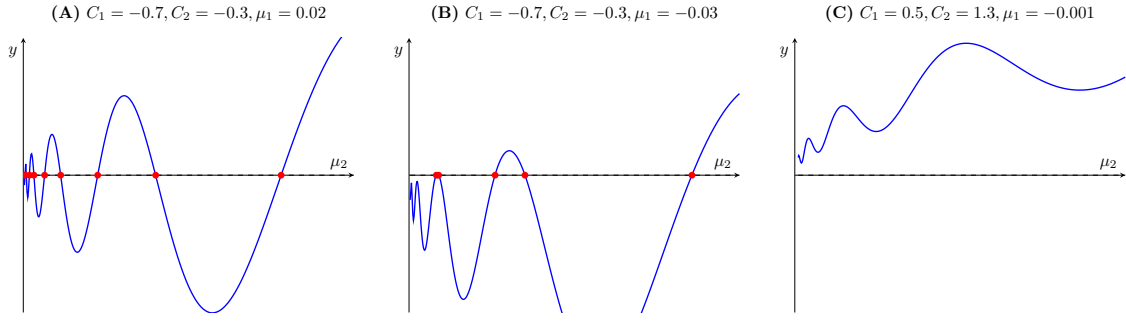
Figure 4.6: Plots of $G(\mu)$ against μ_2 for fixed μ_1, C_1 and C_2. The blue curve is $y = G(\mu)$ and the red dots indicate non-trivial solutions to the equation $G(\mu) = 0$, which correspond to parameter values where secondary homoclinic curves exist. In **(A)** we see infinitely many non-trivial solutions, in **(B)** we see finitely many non-trivial solutions and in **(C)** we see no non-trivial solution, for small values of μ_2.

(S.1) There are independent secondary homoclinic curves which form horizontal *parabolas* and these parabolas approach the primary homoclinic curve $\mu_2 = 0$ asymptotically.

(S.2) These parabolas possess *turning* points where the two corresponding secondary homoclinic branches collide and disappear. The sequence of turning points obtained from successive parabolas appear to approach the origin asymptotically.

(S.3) For different values of C_1 and C_2, the sequence of turning points exist strictly either in the first or second quadrant.

4.2.1   Asymptotics

The observations above can be explained to some extent by obtaining asymptotic expressions for the parabolas and the corresponding turning points.

'Parabolas'

From (4.33), we have

$$\mu_2 + C_1 \mu_2^\nu \sin\left(-\frac{1}{\beta}\log\mu_2\right) + C_2 \mu_2^{\nu + \mu_1/\beta} = 0. \tag{4.34}$$

Also, $\mu_2 > 0$. Let

$$-\frac{1}{\beta}\log\mu_2 = \pi n + \theta,$$

for $n \in \mathbb{N}$ large and $\theta \in (-\pi/2, \pi/2)$. On dividing both sides by μ_2^ν, (4.34) becomes

$$e^{-(1-\nu)\beta(\pi n + \theta)} + (-1)^n C_1 \sin\theta + C_2 e^{(-\mu_1(\pi n + \theta))} = 0. \tag{4.35}$$

As $\nu < 1$, the first term in (4.35) is relatively small for large n. Thus we consider only the leading terms, which gives

$$(-1)^n C_1 \sin\theta + C_2 e^{-\mu_1(\pi n + \theta)} = 0,$$

$$\implies \sin\theta \approx (-1)^{n+1}\frac{C_2}{C_1}e^{-\mu_1 \pi n}, \tag{4.36}$$

for n sufficiently large. We observe that it is not always possible to find solutions θ to (4.36). Suppose $|C_2| > |C_1|$. Then, solutions of (4.36) would only exist if $\mu_1 > 0$. Thus, the set of secondary homoclinic curves would exist only in the first quadrant. If $|C_2| < |C_1|$, solutions of (4.36) can exist for $\mu_1 < 0$, but for $|\mu_1|$ sufficiently small, because of the exponential term.

(A) Continuation

(B): $C_1 = 1.3$, $C_2 = -0.7$, $k = 15, 16..., 90$

(C) Convergence: $C_1 = 1.3$, $C_2 = -0.7$
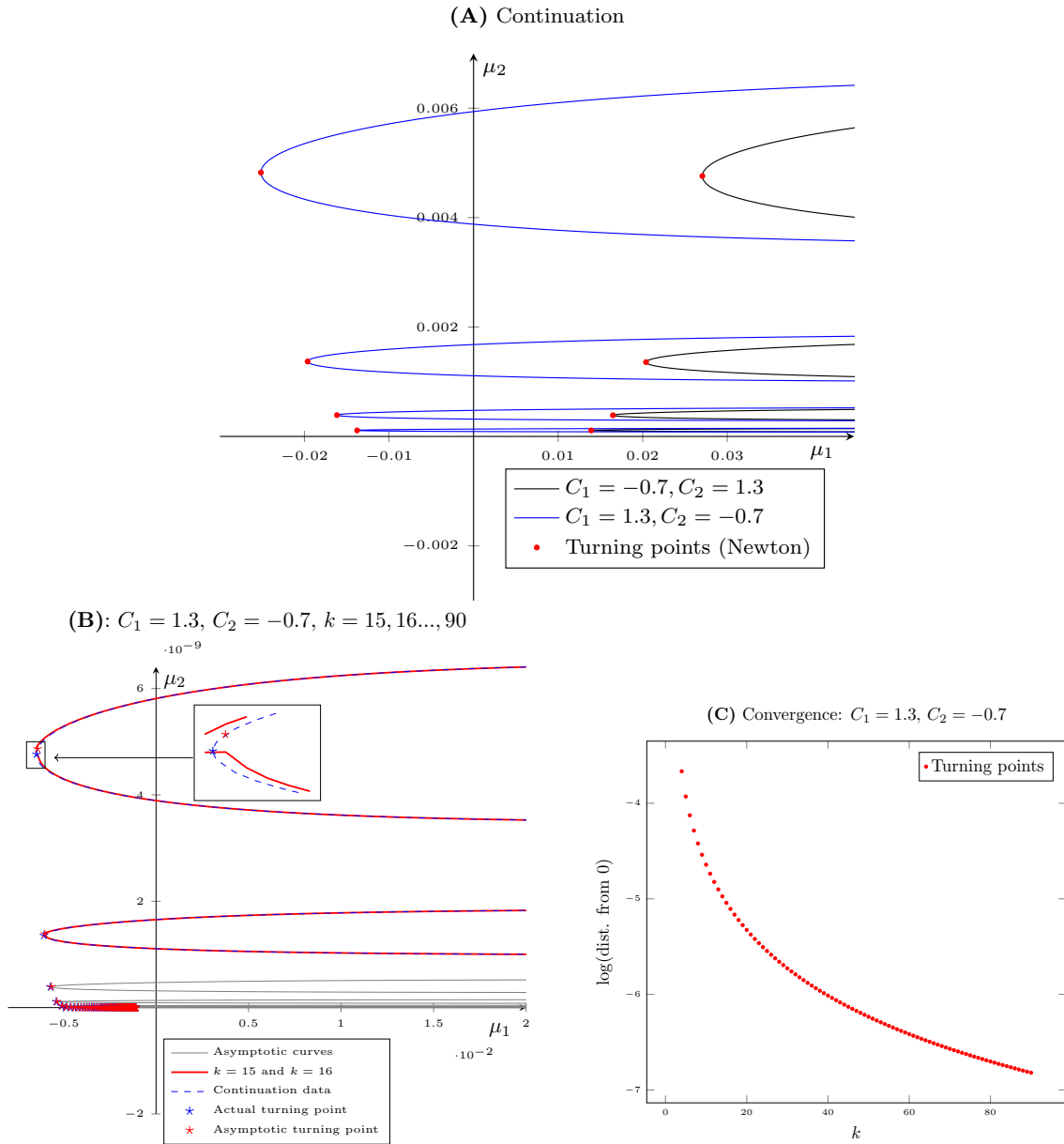
Figure 4.7: Secondary homoclinics near the 3DL bifurcation in the wild case ($\nu < 1$). In **(A)**, multiple secondary homoclinic curves are obtained via continuation in Matcont, for two sets of parameter values. The exact turning points (red points) are obtained by performing Newton iterations starting from asymptotic turning points. The corresponding values of k are $k = 4, 5, 6, 7$. In **(B)**, exact turning points (blue stars) are plotted along with the corresponding asymptotic curves. The corresponding values of k are $k = 15, 16, .90$. We observe that there are discontinuities in the asymptotic curves. This happens when $|\sin\theta| > 1$, where $\sin\theta$ is obtained from (4.43). In **(C)**, the distances of turning points from the origin (3DL bifurcation) are plotted against k, in log scale. Here also, the values of k are $k = 4, 5, .90$.

This also implies that for $|C_2| > |C_1|$, the turning points would exist entirely in the first quadrant, and in the case $|C_2| < |C_1|$, the turning points would be located entirely in the second quadrant. This explains observation **(S.3)**.

From (4.36), we get the following set of branches,

$$\boxed{\mu_2 = e^{(-\beta(\pi n + \theta))},}$$
(4.37)

where $\sin \theta = (-1)^{n+1} \frac{C_2}{C_1} e^{-\pi n \mu_1}$.

For each n, we get a branch that is strictly increasing or decreasing. Two branches corresponding to consecutive values of n combine to form one asymptotic approximation of the parabola. This can be seen directly from the derivative

$$\frac{\partial}{\partial \mu_1} e^{-\beta(\pi n + \theta)} = \underbrace{-\beta}_{<0} \overbrace{e^{-\beta(\pi n + \theta)}}^{>0} \overbrace{\frac{1}{\sqrt{1-\theta^2}}}^{>0} \underbrace{(-1)^n \frac{C_1}{C_2}}_{\pm 1} \overbrace{\pi n}^{>0} \overbrace{e^{-\mu_1 \pi n}}^{>0}.$$
(4.38)

Upon increasing n, the corresponding branches get closer to the axis $\mu_2 = 0$. To approximate the parabola, we choose

$$n_1 = 2k,$$
$$n_2 = 2k - \operatorname{sgn}(C_1/C_2),$$
(4.39)

where $k \in \mathbb{N}$, to get one asymptotic secondary homoclinic curve.

Clearly as $n \to \infty$, the corresponding asymptotic branches $\mu_2^{(n)} = e^{-\beta(\pi n + \theta)}$ approach $\mu_2 = 0$, which is the curve of primary homoclinic curves. Thus observation **(S.1)** can be explained.

In Figure 4.7 **(B)**, asymptotic curves along with two successive curves from continuation are plotted together. The asymptotics agree well with actual continuation curves. However, we observe discontinuities in the asymptotic curves, close to the turning point. This happens when there exists no real solution to (4.43), i.e. when $|\sin \theta| > 1$.

Turning points

It is possible to get the sequence of turning points by solving the defining system by Newton iterations. However, deriving the asymptotics for the turning points gives explanation to observation **(S.2)**.

From (4.34) we have

$$\mu_2 + C_1 \mu_2^\nu \sin\left(-\frac{1}{\beta} \log \mu_2\right) + C_2 \mu_2^{\nu + \mu_1/\beta} = 0,$$
$$\implies 1 + C_1 \mu_2^{\nu-1} \sin\left(-\frac{1}{\beta} \log \mu_2\right) + C_2 \mu_2^{\nu + \mu_1/\beta - 1} = 0,$$
(4.40)

as $\mu_2 \neq 0$. The condition for the turning point is

$$\frac{d}{d\mu_2} \mu_1(\mu_2) = 0.$$

Taking the total derivative of $G(\mu) = 0$ with respect to μ_2 we get

$$\frac{d}{d\mu_2} G(\mu) = 0,$$
$$\implies \frac{\partial}{\partial \mu_1} G(\mu) \underbrace{\frac{d}{d\mu_2} \mu_1}_{=0} + \frac{\partial}{\partial \mu_2} G(\mu) = 0,$$

$$\implies (\nu - 1)C_1 \sin\left(-\frac{1}{\beta}\log\mu_2\right) - \frac{C_1}{\beta}\cos\left(-\frac{1}{\beta}\log\mu_2\right) + C_2(\nu + \mu_1/\beta)\mu_2^{\mu_1/\beta} = 0. \quad (\because \mu_2^{\nu-1} \neq 0)$$

$$(4.41)$$

We separate the various solutions by letting

$$-\frac{1}{\beta}\log\mu_2 = \pi n + \theta,$$

for $n \in \mathbb{N}$ and $\theta \in (-\pi/2, \pi/2)$. The substitution gives us

$$(-1)^n C_1 \left((\nu - 1)\sin\theta - \frac{1}{\beta}\cos\theta\right) + C_2(\nu + \mu_1/\beta)e^{-\mu_1(\pi n + \theta)} = 0,$$

$$\implies \sin\theta - \frac{1}{\beta(\nu - 1)}\cos\theta = (-1)^{n+1}\frac{C_2}{C_1}\underbrace{\frac{(\nu + \mu_1/\beta)}{\nu - 1}}_{\approx \frac{\nu}{\nu-1}}\underbrace{e^{-\mu_1(\pi n + \theta)}}_{\approx 1},$$

$$\implies \sin\theta - \frac{1}{\beta(\nu - 1)}\cos\theta = (-1)^{n+1}\frac{C_2}{C_1}\frac{\nu}{\nu - 1}, \tag{4.42}$$

for μ_1 sufficiently small. From here we derive the expression for $\sin\theta$,

$$\sin\theta \approx \pm\frac{\sqrt{C_1^2\left(\beta^2(\nu - 1)^2 + 1\right) - \beta^2\nu^2 C_2^2}}{C_1\left(1 + \beta^2(\nu - 1)^2\right)},$$

where the $O(\beta^2\nu^2)$ terms were dropped from the numerator. Without loss of generality, we choose θ such that $\sin\theta > 0$. Thus,

$$\boxed{\theta = \arcsin\left(\frac{\sqrt{C_1^2\left(\beta^2(\nu - 1)^2 + 1\right) - \beta^2\nu^2 C_2^2}}{|C_1|\left(1 + \beta^2(\nu - 1)^2\right)}\right).} \tag{4.43}$$

Now that we have θ, we can use (4.34) to get μ_1. Replacing the expression for μ_2 in terms of θ and n in (4.34) gives

$$e^{-(1-\nu)\beta(\pi n + \theta)} + (-1)^n C_1 \sin\theta + C_2 e^{-\mu_1(\pi n + \theta)} = 0,$$

$$\implies -\frac{1}{C_2}e^{-(1-\nu)\beta(\pi n + \theta)} + (-1)^{n+1}\frac{C_1}{C_2}\sin\theta = e^{-\mu_1(\pi n + \theta)}, \tag{4.44}$$

where θ is obtained from (4.43). As the RHS is positive, we need to choose values of n in such a way that the term is always positive. As $e^{-(1-\nu)\beta(\pi n + \theta)}$ is small for n sufficiently large, the LHS of (4.44) is dominated by the sine term and we can determine the sign of the LHS by looking at the sign of C_1/C_2. Thus, we require

$$(-1)^{n+1}\frac{C_1}{C_2} > 0. \tag{4.45}$$

From this we get the expression for n:

$$\boxed{n = 2k + \frac{1}{2}\left[1 + \text{sgn}\left(\frac{C_1}{C_2}\right)\right],} \tag{4.46}$$

where $k \in \mathbb{N}$. By choosing n as above, the LHS of (4.44) is positive and real solutions can be obtained. Continuing the derivation from (4.44), we take the natural logarithm on both sides to get

$$\mu_1 = \frac{-1}{(\pi n + \theta)}\log\left[\frac{-1}{C_2}\left(e^{-(1-\nu)\beta(\pi n + \theta)} + (-1)^n C_1 \sin\theta\right)\right].$$

To summarise, the sequence of asymptotic turning points $\left(\mu_1^{(n)}, \mu_2^{(n)}\right)$ is given by,

$$\boxed{\begin{pmatrix}\mu_1^{(n)} \\ \mu_2^{(n)}\end{pmatrix} = \begin{pmatrix}\frac{-1}{(\pi n + \theta)}\log\left[\frac{-1}{C_2}\left(e^{-(1-\nu)\beta(\pi n + \theta)} + (-1)^n C_1 \sin\theta\right)\right] \\ e^{-\beta(\pi n + \theta)}\end{pmatrix},} \tag{4.47}$$

where $n = 2k + \frac{1}{2}\left[1 + \mathrm{sgn}\left(\frac{C_1}{C_2}\right)\right]$ and θ is obtained from (4.43).

As $n \to \infty$, the sequence (4.47) converges to $(\mu_1, \mu_2) = (0, 0)$. Thus we conclude that the turning points indeed approach the 3DL bifurcation point $\mu = 0$ asymptotically. This explains observation **(S.2)**.

Note that (4.41) along with (4.33) form the defining system for the turning points. With suitable scaling of the variables μ_1 and μ_2, it is possible to obtain the exact turning points via Newton iterations, by starting the iterative procedure at the asymptotic turning points, given by (4.47). The turning points presented in Figure 4.7 are obtained this way.

Chapter 5

Analysing the 3D model map

In this chapter we collect bifurcations of periodic orbits observed close to the 3DL transition as described by the full 3D model map (3.7). The results are similar to that of the scalar model map, except for higher dimensional codimension 2 points that are observed in the 3D case. These points numerically appear to approach the 3DL transition point asymptotically.

We also observe that presence of spring (saddle) areas do not occur for the same parameter values of C_1 and C_2 in the 3D map as they do in the scalar case.

Observations from continuation

Let us define

$$
G(x, \mu) : \begin{pmatrix} x_1 \\ x_2 \\ x_4 \end{pmatrix} \mapsto \begin{pmatrix} 1 + \alpha_1 x_1 x_4^\nu \cos\left(\frac{-1}{\beta} \log x_4 + \phi_1\right) + \alpha_2 x_2 x_4^{\nu + \mu_1/\beta} \\ 1 + \alpha_3 x_1 x_4^\nu \sin\left(\frac{-1}{\beta} \log x_4 + \phi_2\right) + \alpha_4 x_2 x_4^{\nu + \mu_1/\beta} \\ \mu_2 + C_1 x_1 x_4^\nu \sin\left(\frac{-1}{\beta} \log x_4\right) + C_2 x_2 x_4^{\nu + \mu_1/\beta} \end{pmatrix}.
\tag{5.1}
$$

We look for fixed points of this map and the various codimension 1 curves, as we did with the scalar model map (3.10). In Figure 5.1, we see the PD and LP curves obtained from continuation of this map for a chosen set of parameters. Here $C_1 = -1$, $C_2 = 1$, $\alpha_i = 1, \forall i$ and $\phi_1 = \phi_2 = \pi/6$. We immediately observe similarities with respect to the scalar case:

1. We can see that the global structure of these curves is the same as in the scalar case. We also observe spring and saddle areas as in the scalar case.

2. The PD and LP horns are accompanied by Cusp points and/or GPD points (depending on saddle or spring area).

3. The horn structure repeats itself and accumulates onto the primary homoclinic curve $\mu_2 = 0$, as in the scalar case.

This is expected as the scalar map is an asymptotic representation of the 3-dimensional case.

However there are two main differences with respect to the scalar model map which can be attributed to the higher dimension of the 3D map:

1. There exists two NS curves in a very small domain between the PD and LP curves. The end points of the NS segment are *resonance* points.

2. Along the PD, LP and NS curves we observe many higher dimensional codimension 2 points. These points are:

   - Cusp: Along the LP curve.
   - GPD (Generalised Period Doubling): Along the PD curve (only in the case of spring area).

- R1:1 (Resonance 1:1): Along the PD curve.
- R1:2 (Resonance 1:2): Along the LP curve.
- LPPD (Fold-Flip): Along the LP curve.
- R1:3 (Resonance 1:3): Along the NS curve.
- R1:4 (Resonance 1:4): Along the NS curve.

These points appear to numerically approach the origin $\mu = 0$ (3DL transition). The endpoints of the NS curve are points R1 and R2, as can be seen in Figure 5.1 **(B)**. For a detailed discussion on the various codimension 2 points and their normal forms, see [12].

We do not observe a significant difference in the behaviour of the PD/LP curves upon changing the coefficients α_i and ϕ_j. This can be attributed to the effect of the corresponding terms in (5.1) to the dynamics of x_4. These terms are $O(\|x\|^{2\nu})$ in the fixed point equation for x_4.

Codimension 2 points along LP, PD and NS curves

As stated before, there exist multiple codimension 2 points along the PD, LP and NS curves. These points appear to approach the origin $\mu = 0$ asymptotically. In Figure 5.2 we present the sequence of codimension 2 points found on successive PD/LP curves of Figure 5.1. These sequences are obtained via detection along PD/LP curves from continuation. GPD points are absent as they are generally hard to detect along continuations, due to large test function values and absolute gradients. They are approximated in practice by noting where the sign of the scalar GPD test function changes.

Note that codimension 2 points such as R1, R2 and LPPD were observed more than once on a single PD/LP curve. The tables for each detection is computed separately.

Spring and saddle areas

For the scalar map we observed that there exist transitions between spring and saddle areas. These transitions can be explained by observing the appearance and disappearance of GPD points, as they exist generically on the PD loop in a spring area, and do not exist in the case of a saddle area.

In the 3D case too, we numerically observe such transitions. However when there is a spring (saddle) area in the 3D case, it does not imply that the same structure would exist in the 1D map for the same choice of parameters C_1 and C_2. This is shown in Figure 5.3.
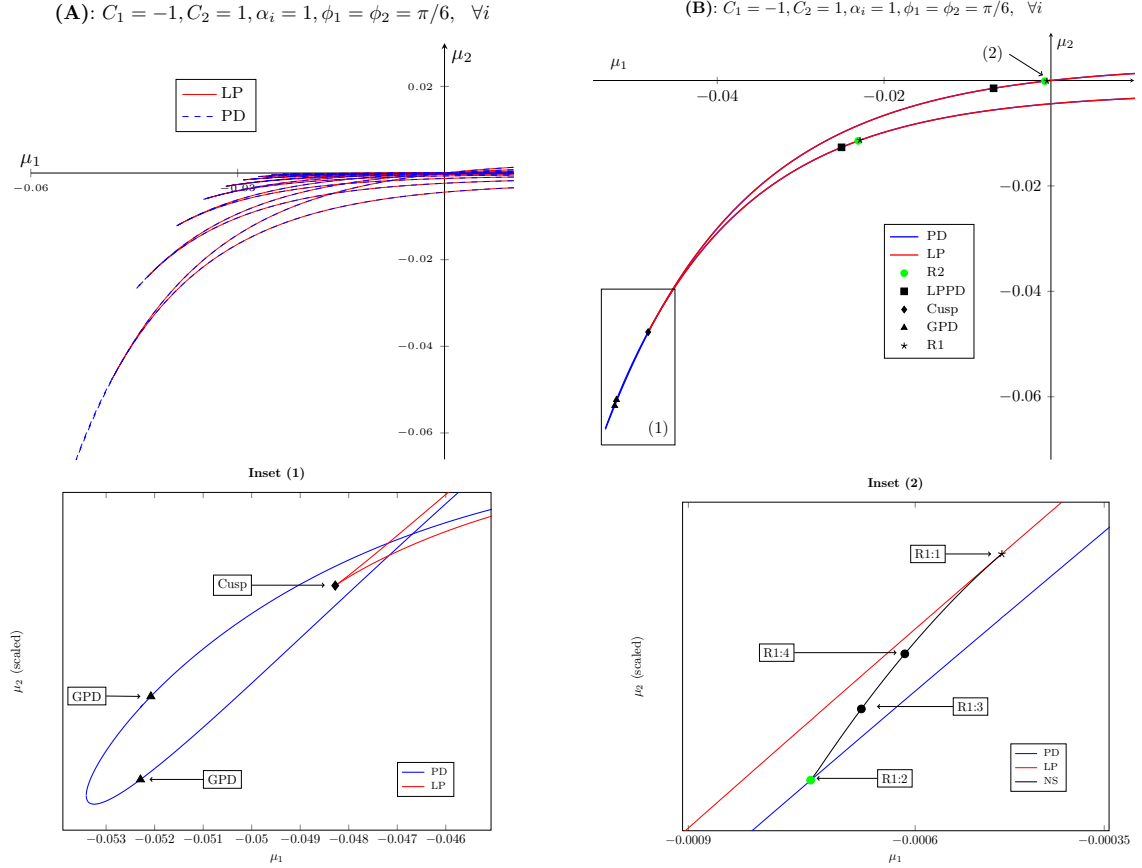
Figure 5.1: Primary PD and LP curves obtained by continuation, for the map (5.1) for a fixed choice of parameters C_1 and C_2. The curves have almost the same global structure, as can be seen in **(A)**. In **(B)** we see one such curve, along with the multiple codimension 2 points that are found along it. In Inset (1) we see the previously described spring area made up by the PD and LP curves. Three codimension 2 bifurcation points are observed, two corresponding to the generalised period doubling (GPD) bifurcation and one corresponding to the Cusp bifurcation. In Inset (2) we see the interaction between the 1:2 resonance (R2) point on the PD curve and the 1:1 resonance point on the LP curve, via the primary NS curve. On this curve we find two more codimension 2 bifurcation points, 1:3 resonance (R3) and 1:4 resonance (R4).

Table 5.1: Cusp

μ_1	μ_2
-0.04827775	-0.04773564
-0.04285354	-0.02357456
-0.03838913	-0.01179054
-0.03471637	-0.00596640
-0.03166789	-0.00304826
-0.02910762	-0.00156918
-0.02693127	-0.00081256
-0.02506011	-0.00042273
-0.02343464	-0.00022073
-0.02200947	-0.00011560

Table 5.2: R1 (1)

μ_1	μ_2
-0.022885016	-0.011329596
-0.020339780	-0.005892797
-0.018309568	-0.003084872
-0.016651283	-0.001621763
-0.015270744	-0.000855070
-0.014103227	-0.000451779
-0.013102731	-0.000239073
-0.012235644	-0.000126665
-0.011476831	$-6.7172703 \cdot 10^{-5}$
-0.010807113	$-3.5650007 \cdot 10^{-5}$

Table 5.3: R1 (2)

μ_1	μ_2
-0.000491070	$-5.2368318 \cdot 10^{-5}$
-0.000485291	$-8.9357361 \cdot 10^{-5}$
-0.000472811	$-2.924643 \cdot 10^{-5}$
-0.000446309	$-1.5962248 \cdot 10^{-5}$
-0.000418299	$-8.611892 \cdot 10^{-6}$
-0.000391533	$-4.6189982 \cdot 10^{-6}$
-0.000366963	$-2.4699226 \cdot 10^{-6}$
-0.000344774	$-1.3186873 \cdot 10^{-6}$
-0.000324856	$-7.0350767 \cdot 10^{-7}$
-0.000306980	$-3.7517618 \cdot 10^{-7}$

Figure 5.2: Table of codimension 2 points found along successive PD/LP curves for $C_1 = -1, C_2 = 1, \alpha_i = 1, \phi_1 = \phi_2 = \pi/6, \forall i$.

Table 5.4: R2 (1)

μ_1	μ_2
-0.023104053	-0.011454847
-0.020441356	-0.005925675
-0.018357592	-0.003093697
-0.016674314	-0.001624164
-0.015281911	-0.000855730
-0.014108689	-0.000451962
-0.013105423	-0.000239124
-0.012236979	-0.000126679
-0.011477496	$-6.7176657 \cdot 10^{-5}$
-0.010807446	$-3.5651115 \cdot 10^{-5}$

Table 5.5: R2 (2)

μ_1	μ_2
-0.000734733	-0.000134556
-0.000610792	$-6.5156479 \cdot 10^{-5}$
-0.000530855	$-3.2871209 \cdot 10^{-5}$
-0.000474690	$-1.6990978 \cdot 10^{-5}$
-0.000432269	$-8.9039388 \cdot 10^{-6}$
-0.000398451	$-4.7019541 \cdot 10^{-6}$
-0.000370410	$-2.4935164 \cdot 10^{-6}$
-0.000346506	$-1.3254274 \cdot 10^{-6}$
-0.000325720	$-7.0541284 \cdot 10^{-7}$
-0.000307415	$-3.7571786 \cdot 10^{-7}$

Table 5.6: LPPD (1)

μ_1	μ_2
-0.025100238	-0.012679658
-0.022290657	-0.006566350
-0.020062324	-0.003428503
-0.018247704	-0.001799398
-0.016739195	-0.000947643
-0.015464156	-0.000500275
-0.014371585	-0.000264567
-0.013424514	-0.000140101
-0.012595437	$-7.4267094 \cdot 10^{-5}$
-0.011863435	$-3.9401153 \cdot 10^{-5}$

Table 5.7: LPPD (2)

μ_1	μ_2
-0.006872844	-0.001480276
-0.006187132	-0.000783903
-0.005623142	-0.000415956
-0.005152068	-0.000220997
-0.004753167	-0.000117515
-0.004411273	$-6.2525452 \cdot 10^{-5}$
-0.004115103	$-3.3281613 \cdot 10^{-5}$
-0.003856121	$-1.7721099 \cdot 10^{-5}$
-0.003627768	$-9.4381076 \cdot 10^{-6}$
-0.003424932	$-5.0276577 \cdot 10^{-6}$

Figure 5.2 (Cont.): Table of codimension 2 points found along successive PD/LP curves for $C_1 = -1, C_2 = 1, \alpha_i = 1, \phi_1 = \phi_2 = \pi/6, \forall i$.
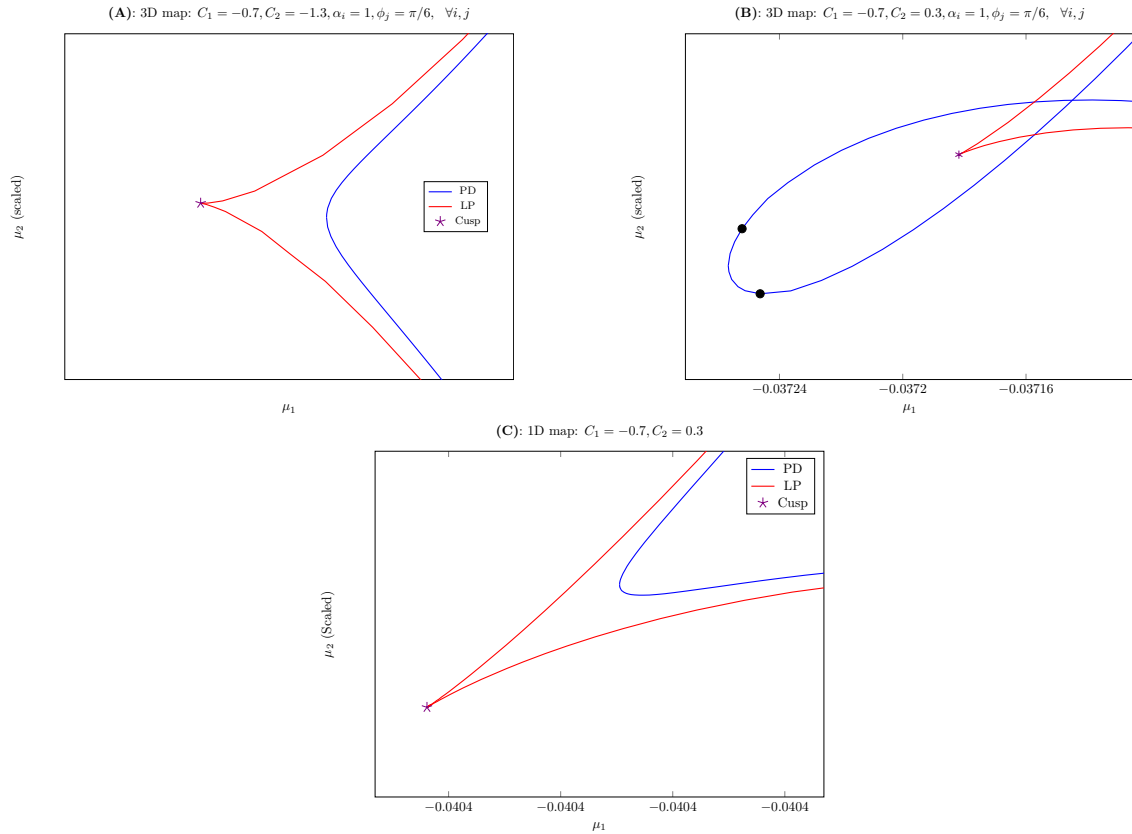
Figure 5.3: Plots of spring and saddle areas in the scalar map (3.10) and 3D map (3.7). In all plots μ_2 is scaled for convenience. In **(A)** we see that there exists a saddle area in the 3D case, where GPD points are absent. **(B)** and **(C)** are plotted for the same value of C_1 and C_2, but with respect to the 3D map (3.7) and 1D map (3.10) respectively. We see that the existence of the spring area in the 3D map does not imply the existence of the same in the 1D map.

Chapter 6

Discussion and outlook

In this chapter we collect all results on the 3DL bifurcation together and note the differences and similarities to the Belyakov case. We also highlight some of the ideas that can be explored ahead to make the understanding of this bifurcation richer.

6.1 Novelties

The 3DL bifurcation is a codimension 2 bifurcation that occurs generically in 4D systems. From the Homoclinic Center Manifold theorem we know that this bifurcation may also be observed in systems with dimension $n \geq 4$. It is characterised by the transition from a saddle to saddle-focus along a two-parameter curve of primary homoclinic orbits in such a way that at the transition, the critical stable (unstable) leading eigenspace is three dimensional, making it different from the Belyakov case.

By considering a generic 4D system with 3DL transition, we are able to obtain a two-parameter model return map which describes the bifurcations occurring close to the transition. Analysis of fixed points of these model maps gives information of global bifurcations occurring close to the transition in the ODE system. We see that when the saddle index ν is less than 1, there exist infinitely many bifurcation curves. We concentrate only on the bifurcation sets obtained in the case $\nu < 1$ (wild case). The model maps (equations) describe the following bifurcations:

- Period Doubling (PD) bifurcation.

- Limit Point (LP) bifurcation.

- Secondary homoclinic bifurcation.

We have the following model maps (equations):

$$\Pi(x,\mu) : \begin{pmatrix} x_1 \\ x_2 \\ x_3 \end{pmatrix} \mapsto \begin{pmatrix} 1 + \alpha_1 x_1 (x_3)^\nu \cos\left(\frac{-1}{\beta}\log x_3 + \phi_1\right) + \alpha_2 x_2 (x_3)^{\nu + \mu_1/\beta} \\ 1 + \alpha_3 x_1 (x_3)^\nu \sin\left(\frac{-1}{\beta}\log x_3 + \phi_2\right) + \alpha_4 x_2 (x_3)^{\nu + \mu_1/\beta} \\ \mu_2 + C_1 x_1 (x_3)^\nu \sin\left(\frac{-1}{\beta}\log x_3\right) + C_2 x_2 (x_3)^{\nu + \mu_1/\beta} \end{pmatrix}, \qquad (6.1)$$

and

$$F(x,\mu) : x \mapsto \mu_2 + C_1 x^\nu \sin\left(-\frac{1}{\beta}\log x\right) + C_2 x^{\nu + \mu_1/\beta}, \qquad (6.2)$$

that describe bifurcations of periodic orbits (PD, LP and NS) and

$$G(\mu_2) = \mu_2 + C_1 \mu_2^\nu \sin\left(-\frac{1}{\beta}\log \mu_2\right) + C_2 \mu_2^{\nu + \mu_1/\beta} = 0, \qquad (6.3)$$

that describes secondary homoclinic bifurcations. Here μ_1 controls the eigenvalue configurations and the homoclinic connection exists only for $\mu_2 = 0$. For $\mu_1 < 0$ we have the saddle case, for
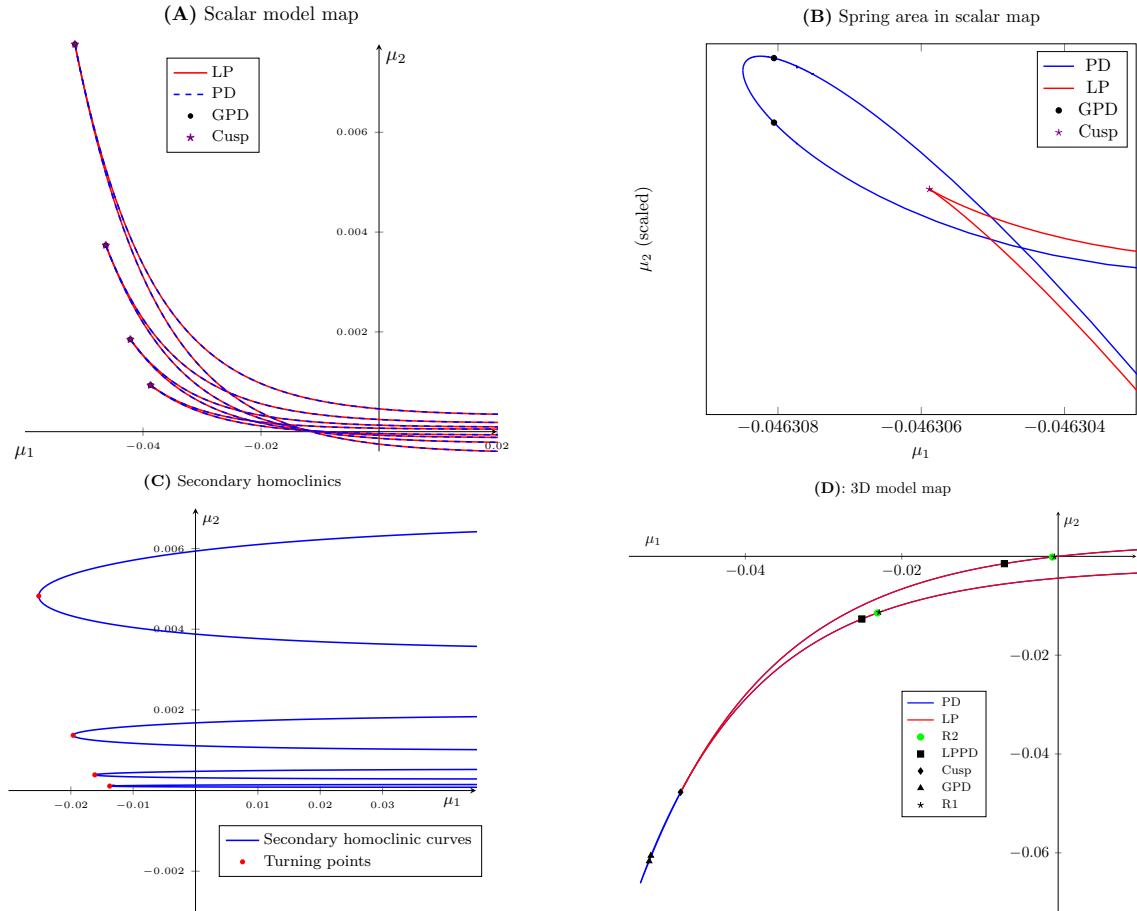
Figure 6.1: Summary of bifurcations occurring close to the 3DL transition. μ_1 controls the eigenvalue configuration. For $\mu_1 < 0$ we have the saddle case, for $\mu_1 = 0$ we have the 3DL saddle and for $\mu_1 > 0$ we have the saddle-focus case. The primary homoclinic connection exists only when $\mu_2 = 0$. In **(A)** PD and LP 'horns' of the scalar model map are plotted. In **(B)** the spring area at the tip of the horn is shown. In **(C)** secondary homoclinic 'parabolas' and their corresponding turning points are plotted. In **(D)** a single PD/LP horn of the 3D model map is plotted, along with several codimension 2 points found along it.

$\mu_1 = 0$ we are at the 3DL transition and for $\mu_1 > 0$ we have the saddle-focus case. These maps (equations) are very different from the known model maps (equations) in the saddle, saddle-focus or Belyakov cases. The presence of the additional term $C_2 x^{\nu + \mu_1/\beta}$ in (6.2) is the most significant difference from all other model maps.

In Figure 6.1 some of the bifurcation curves with respect to parameters μ_1 and μ_2 are plotted. We make the following observations:

(3DL.1) There exist infinitely many PD, LP, NS and secondary homoclinic curves, that accumulate onto the curve of primary homoclinic orbits.

(3DL.2) Each PD and LP curve has a 'horn' composed of two branches. Close to the horn's turning point these two curves interact via spring and saddle areas. Transitions between saddle and spring areas are observed upon changing parameters C_1 and C_2. Each secondary homoclinic curve forms a horizontal parabola. These parabolas may exist only in the quadrant $\{\mu_1 > 0, \mu_2 > 0\}$ depending on parameters C_1 and C_2.

(3DL.3) Several codimension 2 points are found along each of the PD, LP and NS curves. In the scalar case, we observe GPD (along PD) and cusp (along LP) points. Secondary homoclinic curves have turning points where two secondary homoclinic orbits collide and disappear. In the 3D case we observe:

- Cusp (along LP).
- GPD (along PD).
- fold-flip (along PD and LP).
- Resonance 1:1 (along LP).
- Resonance 1:2 (along PD).
- Resonance 1:3 (along NS).
- Resonance 1:4 (along NS).

We were able to prove in the scalar case analytically that the cusp points asymptotically approach the 3DL transition point. The same is done in the case of secondary homoclinic turning points. In the 3D model map it appears numerically that all the above codimension points approach the 3DL transition point.

(3DL.4) When μ_1 is fixed to be negative (saddle case), there exist only finitely many bifurcation curves for μ_2 sufficiently small. However, when μ_1 is fixed as positive (saddle-focus case), there exist infinitely many bifurcation curves for μ_2 sufficiently small. This is analogous to the saddle and saddle-focus homoclinic bifurcations, where single and infinitely many periodic orbits emerge respectively. This highlights the robustness of the model map.

Limitations of a model map

It must be noted that the formulation of the model map is based on obtaining C^1 equivalence to the linear system due to Belitskii's theorem. In principle we can only trust results based on first derivatives, such as the PD and LP curves, and not cusp points, for example, which are based on third derivatives of the map. However this can be worked around in two ways:

- We can impose non-resonant conditions

$$\mathrm{Re}\lambda_i \neq p\,\mathrm{Re}\lambda_j + q\,\mathrm{Re}\lambda_k,$$

  where λ's are eigenvalues and $p, q > 1$. This increases the smoothness of the equivalence and we can proceed with the treatment which would be valid generically.

- We can try to prove that the model map derived in the Thesis correctly approximates the actual Poincaré map close to the critical saddle in (3.1).

We will leave these matters for future work.

6.2 3DL transition and the Belyakov bifurcation

In the previous section we mentioned that the 3DL transition is different from the Belyakov transition. But how so?

As mentioned in Chapter 1, the Belyakov transition is the only other analysed saddle to saddle-focus transition. This occurs generically in a 3D system. A pair of leading stable (unstable) complex eigenvalues approach the real axis and split into two distinct real eigenvalues. At the transition point, there exists a double real stable leading eigenvalue.

This is different from the 3DL case where the pair of complex eigenvalues exchange their position relative to the real eigenvalue such that at the critical parameter values there exists a three dimensional stable (unstable) leading situation at the transition point. This occurs generically in a 4D system.

There are further more differences in the bifurcation sets close to the transition point. To motivate them we introduce the model return map in the Belyakov case and the bifurcation diagram in the case of PD, LP and secondary homoclinic cases.

The model map in the case of the Belyakov bifurcation is 2-dimensional and can further be reduced to a scalar map. The two maps are:

$$\Pi_B : \begin{pmatrix} y_1 \\ y_2 \end{pmatrix} \mapsto \begin{pmatrix} 1 + \frac{A}{\sqrt{\mu_1}} y_1 y_2^\rho \cos\left(-\frac{\sqrt{\mu_1}}{\lambda} \ln y_2 + \Theta\right) \\ \mu_2 + \frac{B}{\sqrt{\mu_1}} y_1 y_2^\rho \sin\left(-\frac{\sqrt{\mu_1}}{\lambda} \ln y_2\right) \end{pmatrix}, \tag{6.4}$$

and

$$F_B(y, \mu) : y \mapsto \mu_2 + \frac{B}{\sqrt{\mu_1}} y^\rho \sin\left(-\frac{\sqrt{\mu_1}}{\lambda} \ln y\right). \tag{6.5}$$

Here μ_1 is non-negative and controls the eigenvalue configurations. μ_2 controls the existence of the primary homoclinic connection. For $\mu_1 = 0$ we are at the Belyakov bifurcation (double real eigenvalue) and for $\mu_1 > 0$ we have complex leading stable eigenvalues. The primary homoclinic connection exists for $\mu_2 = 0$ only. A, B and Θ are constants. Note that for secondary homoclinics, the equation is just

$$F_B(\mu_2, \mu) = 0. \tag{6.6}$$

In Figure 6.2 we show the PD, LP and secondary homoclinic bifurcation curves that occur close
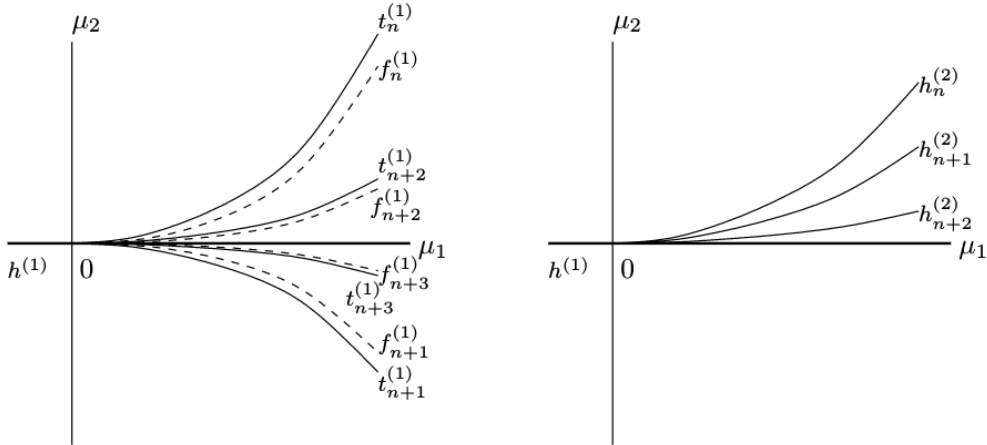
Figure 6.2: Bifurcations sets close to the Belyakov bifurcation (at 0). Here $\{t_n^{(1)}\}$ refers to the set of primary limit point curves, $\{f_n^{(1)}\}$ refers to the set of primary period doubling curves and $\{h_n^{(2)}\}$ refers to the set of secondary homoclinic curves. The parameters μ_1 and μ_2 control the transition of the saddle to the Belyakov case and the appearance of the homoclinic orbit respectively. Figure taken from [13].

to the transition point for maps (6.5) and (6.6). Although we obtain infinitely many PD, LP and secondary homoclinic curves, the structure of these curves is very different from that of the 3DL case. We highlight some of the differences :

1. The curves in the Belyakov case are characterised by single branches which have the same structure for all three bifurcations. These branches do not form local structures like horns, loops or knots. For the 3DL case, these curves behave differently. The PD/LP curves form horns, where the PD curves make sharp turns (spring area) or loops (saddle area) and the LP curves are possess cusps. The secondary homoclinic curves form parabolas.

2. The bifurcation curves in the Belyakov case have no codimension 2 points along them. In the 3DL case we observe GPD and Cusp points in the scalar map, and fold-flip and strong resonances in the 3D case. These codimension 2 points (appear to) approach the 3DL bifurcation point asymptotically.

3. The bifurcation curves have infinite order tangency at the transition point in the Belyakov case and do not exist in the saddle case (when $\mu_1 < 0$). However in the 3DL case these curves exist also when $\mu_1 < 0$. Moreover, most of the interesting localised structures like spring areas, saddle areas and turning points (in the case of secondary homoclinic orbits) occur when $\mu_1 < 0$.

6.3 Unexplored areas

From this Thesis we obtain a model return map which gives us information about primary PD, LP and NS bifurcations, along with secondary homoclinic bifurcations occurring close to the 3DL transition. However there are more ideas that we feel can be explored to obtain knowledge of further more bifurcations occurring close to the saddle.

Higher order periodic orbits and chaotic domains

From the 3D model map (6.1) it would be possible to describe bifurcations of higher order periodic orbits, that make multiple global passages before returning to the equilibrium. It would be interesting to see the structures higher order period doubling curves form, and to see if there exist chaotic domains.

A toy model

So far we describe the bifurcations close to a 3DL transition by means of a model map. However we would also like to find such a transition in a system of ODEs and confirm our results. Either we can try and look for an example in the numerous ODE models constructed for applications in ecology, neuroscience, physics etc. or we can try to construct a toy model. A detailed discussion on constructing ODEs with homoclinic orbits can be found in [6].
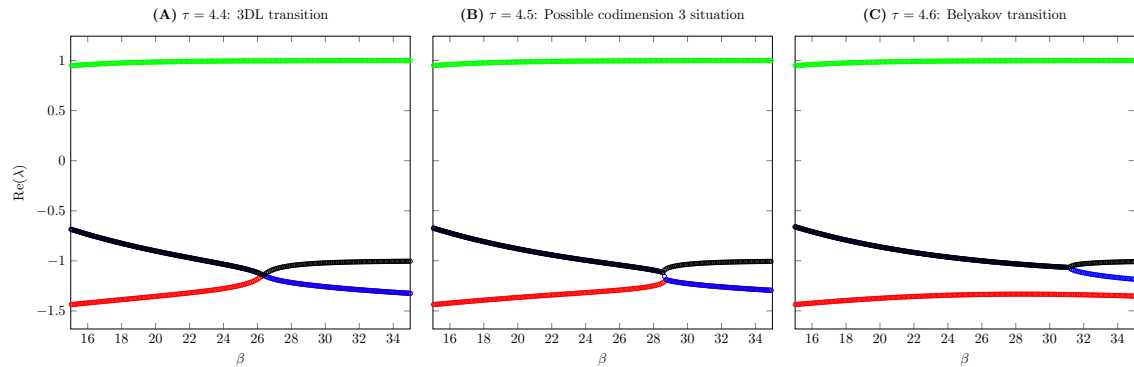
Figure 6.3: A possible 3DL to Belyakov transition as seen in the ODE system (6.7), along a three-parameter continuation (β, c and τ). Here real parts of the 4 eigenvalues are plotted against β, along a curve of primary homoclinic orbits (continued in $\beta - c$). On changing τ, 3DL transition (in figure (**A**)) and Belyakov transition (in figure (**C**)) are observed. Around $\tau \approx 4.5$ (in figure (**B**)), we see that two Belyakov bifurcations occur almost simultaneously, giving rise to a possible triple-real stable leading situation. Continuation performed in Matcont [7].

Belyakov to 3DL transition

In the same way we construct and derive the model map for the 3DL transition, it would be interesting to see if a three-parameter model map describing the Belyakov to 3DL transition can be derived. This codimension 3 situation was also observed in [14] in the tame case ($\nu > 1$). The

corresponding ODE system is,

$$
\begin{cases}
\dot{u} &= -(u - \psi + a)/c, \\
\dot{\phi} &= \phi, \\
\dot{\psi} &= \dfrac{f(u) + f'(u)(-u + \psi + a)/\nu - 2c\phi/\nu - \psi}{c^2/\nu^2 - 1}, \\
\dot{a} &= -(a - \kappa u)/(c\tau),
\end{cases}
\tag{6.7}
$$

where $f(u) = (1 + \exp(\beta(u - \theta))^{-1}$. The parameters $\beta, \tau, \kappa, \theta$ and c are positive, while ν^{-1} is kept zero. Figure 6.3 shows the transition.

References

[1] V. S. Afraimovich, S. V. Gonchenko, L. M. Lerman, A. L. Shil'nikov, and D. V. Turaev. Scientific heritage of L. P. Shilnikov. *Regul. Chaotic Dyn.*, 19(4):435–460, 2014.

[2] A. A. Andronov, E. A. Leontovich, I. I. Gordon, and A. G. Maĭ er. *Theory of Bifurcations of Dynamic Systems on a Plane*. Izdat. "Nauka", Moscow, 1967.

[3] V. I. Arnold, V. S. Afrajmovich, Yu. S. Il'yashenko, and L. P. Shil'nikov. *Dynamical Systems 5: Bifurcation theory and catastrophe theory*. Springer-Verlag, Berlin, 1999.

[4] L. A. Belyakov. The bifurcation set in a system with a homoclinic saddle curve. *Mat. Zametki*, 28(6):911–922, 962, 1980.

[5] L. A. Belyakov. Bifurcations of systems with a homoclinic curve of the saddle-focus with a zero saddle value. *Mat. Zametki*, 36(5):681–689, 798, 1984.

[6] B. Deng. Constructing homoclinic orbits and chaotic attractors. *Internat. J. Bifur. Chaos Appl. Sci. Engrg.*, 4(4):823–841, 1994.

[7] A. Dhooge, W. Govaerts, and Yu. A. Kuznetsov. Matcont: A MATLAB package for numerical bifurcation analysis of odes. *ACM Trans. Math. Softw.*, 29(2):141–164, June 2003.

[8] S. V. Gonchenko, D. V. Turaev, P. Gaspard, and G. Nicolis. Complexity in the bifurcation structure of homoclinic loops to a saddle-focus. *Nonlinearity*, 10(2):409–423, 1997.

[9] W. Govaerts, Yu. A. Kuznetsov, R. Khoshsiar Ghaziani, H.G.E. Meijer, and N. Neirynck. MatcontM: A toolbox for continuation and bifurcation of cycles of maps: Command line use.

[10] A. J. Homburg and B. Sandstede. Homoclinic and heteroclinic bifurcations in vector fields. *Handbook of Dynamical Systems*, 3(C):379–524, 2010.

[11] Yu. Ilyashenko and Weigu Li. *Nonlocal bifurcations*, volume 66 of *Mathematical Surveys and Monographs*. American Mathematical Society, Providence, RI, 1999.

[12] Yu. A. Kuznetsov. *Elements of applied bifurcation theory*, volume 112 of *Applied Mathematical Sciences*. Springer-Verlag, New York, third edition, 2004.

[13] Yu. A. Kuznetsov, O. De Feo, and S. Rinaldi. Belyakov homoclinic bifurcations in a tritrophic food chain model. *SIAM J. Appl. Math.*, 62(2):462–487, 2001.

[14] H. G. E. Meijer and S. Coombes. Travelling waves in a neural field model with refractoriness. *J. Math. Biol.*, 68(5):1249–1268, 2014.

[15] C. Mira and J.-P. Carcassès. On the "crossroad area–saddle area" and "crossroad area–spring area" transitions. *Internat. J. Bifur. Chaos Appl. Sci. Engrg.*, 1(3):641–655, 1991.

[16] L. P. Shil'nikov. A case of the existence of a denumerable set of periodic motions. *Dokl. Akad. Nauk SSSR*, 160:558–561, 1965.

[17] L. P. Shil'nikov, A. L. Shil'nikov, D. V. Turaev, and L. O. Chua. *Methods of qualitative theory in nonlinear dynamics. Part I*, volume 4 of *World Scientific Series on Nonlinear Science. Series A: Monographs and Treatises*. World Scientific Publishing Co., Inc., River Edge, NJ, 1998.